1 **Physical processes influencing the Asian climate due to black carbon emission**

2 **over East and South Asia**

3 *Feifei Luo[1], Bjørn H. Samset[2], Camilla W. Stjern[2], Manoj Joshi[3], Laura J. Wilcox[4],*

4 *Robert J. Allen[5], Wei Hua[1], and Shuanglin Li[6,7]*

5 1. School of Atmospheric Sciences/Plateau Atmosphere and Environment Key

6   Laboratory of Sichuan Province/Meteorological Disaster Prediction and Warning

7   Engineering Laboratory of Sichuan Province, Chengdu University of Information

8   Technology, Chengdu, China

9 2. CICERO Center for International Climate Research, Oslo, Norway

10 3. Climatic Research Unit, School of Environmental Sciences, University of East

11   Anglia, Norwich, United Kingdom

12 4. National Centre for Atmospheric Science, University of Reading, Reading, United

13   Kingdom

14 5. Department of Earth and Planetary Sciences, University of California Riverside,

15   Riverside, CA, United States of America

16 6. Climate Change Research Center, Institute of Atmospheric Physics, Chinese

17   Academy of Sciences, Beijing, China

18 7. Department of Atmospheric Science, China University of Geoscience, Wuhan,

19   China

20 Corresponding author: Feifei Luo (lff@cuit.edu.cn)

21 To be submitted to Atmospheric Chemistry and Physics

Abstract

24   Many studies have shown that black carbon (BC) aerosols over Asia have

25 significant impacts on regional climate, but with large diversities in intensity, spatial

26 distribution and physical mechanism of regional responses. In this study, we utilized a

27 set of Systematic Regional Aerosol Perturbations (SyRAP) using a reduced complexity

28 climate model, FORTE2, to investigate responses of the Asian climate to BC aerosols

29 over East Asia only, South Asia only, and both regions at once, and thoroughly examine

30 related physical processes. Results show that regional BC aerosols lead to a strong

31 surface cooling, air temperature warming in the low-level troposphere, and drying over

32 the perturbed areas, with seasonal differences in magnitude and spatial distribution.

33 Atmospheric energy budget analysis suggests that reductions in local precipitation

34 primarily depend on the substantial local atmospheric heating due to shortwave

35 absorption by BC. Increases in dry static energy (DSE) flux divergence partly offset the

36 reduced precipitation over north China in summer and most of China and India in the

37 other three seasons. Decreases in DSE flux divergence lead to stronger reduction in

38 precipitation over south China and central India in summer. Changes in DSE flux

39 divergence are mainly due to vertical motions driven by diabatic heating in the middle

40 and lower troposphere. BC perturbations also exert non-local climate impacts through

41 the changes in DSE flux divergence. This study provides a full chain of physical

42 processes of the local climate responses to the Asian BC increases, and gives some

43 insights to better understand the uncertainties of model responses.

1. Introduction

Black carbon (BC) aerosol, a short-lived pollutant and climate forcer, is emitted from the incomplete combustion of biomass and fossil fuels, and exerts significant effects on global and regional climate (Ramanathan and Carmichael, 2008; Bond et al., 2013; Stjern et al., 2017; IPCC, 2021; Li et al., 2022). Alongside rapid economic developments of China and India over the past few decades, East and South Asia have become the highest BC emissions hotspots in the world. Despite BC emissions from China decreasing substantially in the past decade, East and South Asia are expected to remain the highest BC loadings globally in the coming decades (Lund et al., 2019). Hence, the climate impacts of BC emissions from East and South Asia have been extensively investigated (e.g. Li et al., 2016; Lou et al., 2019; Xie et al., 2020; Westervelt et al., 2020; Herbert et al., 2022; Yang et al., 2022). Although many model studies have shown that Asian BC aerosols are of great importance for local climate (especially the Asian monsoonal systems), considerable uncertainty exists regarding the intensity and spatial distribution of the Asian climate responses to BC forcings, as well as the related physical mechanisms.

Menon et al. (2002) found that during summer, a large BC forcing induced a "southern flooding and northern drought" (SFND) precipitation pattern in China based on a global climate model (CGCM), and moderate cooling in China and India based on the Goddard Institute for Space Studies (GISS) global climate model (CGCM). In contrast, some subsequent modeling studies found that BC forcing acted to suppress precipitation in However, many subsequent studies were not able to reproduce the SFND pattern, in part due to the poor representation of the Asian summer monsoon in models (Wilcox et al., 2015). Gu et al. (2006) found that BC forcing acted to suppress precipitation in southern and eastern China while strengthening it in the north (Gu et al., 2006; Zhang et al., 2009; Liu et al., 2018). Additionally, some studies suggested that BC aerosols caused a tripolar precipitation pattern with wetting-drying-wetting from north to south China (Mahmood and Li, 2014; Xie et al., 2020), or there was no statistically significant response in precipitation over East China (Jiang et al., 2013; Guo et al., 2013; Wang et al., 2017).due to warming in the middle to high latitudes

based on an atmospheric general circulation model (AGCM). Zhang et al. (2009) showed that the effects of direct radiative forcing due to increased BC aerosols can decrease precipitation and increase surface temperature in southern China and India, but cause the opposite responses in northern China, by comparing CAM3 AGCM simulations with the all aerosol types and without carbonaceous aerosol. Liu et al. (2018) found a similar dipole precipitation pattern with a decrease in southern China and an increase in the north mainly due to the fast adjustments (simulations with fixed SST) of BC forcing, and a surface cooling over Asia except over the Himalayan region in the 10x modern Asian BC emissions or concentrations experiments in the Precipitation Driver Response Model Intercomparison Project (PDRMIP) (Myhre et al., 2017).

Regional precipitation responses to BC aerosols can be attributed to both surface cooling induced by aerosol-radiation interaction (ARI) and atmospheric heating by aerosol absorption (Stier et al., 2024). However, the relative importance of the two effects is debated. Persad et al. (2017) have shown that surface cooling dominates the reduction of the East Asian summer precipitation due to the decreased land-sea thermal contrast, whilst atmospheric heating partially offset the reduction. Xie et al. (2020) have proposed that the precipitation responses mainly result from the upper-level atmospheric heating over Asia, which enhances the upper-level meridional land-sea thermal gradient and subsequently strengthens the low-level monsoon circulation. Wang et al. (2017) conducted CESM1 simulations with increased BC emissions from preindustrial to present-day level, and proposed that the fast adjustment strengthened the EASM, while slow adjustment (response to aerosol-induced SST change) dominated the spatial pattern of precipitation response, which showed a tripolar precipitation pattern with wetting-drying-wetting from north to south China, although the responses in most regions were statistically insignificant. The fast/slow responses in Wang et al. (2017) are different with those in Liu et al. (2018). Xie et al. (2020) used the PDRMIP ensemble to show that the extremely high global/Asian BC forcing can cause the similar tripolar precipitation pattern over eastern China in summer, and they

stressed that these responses mainly result from the enhanced upper-level atmospheric temperature over Asia instead of low-level thermal feedbacks. Mahmood and Li (2014) showed that South Asian BC also can induce the tripolar precipitation pattern over East China via a propagating wave train along the Asian upper tropospheric jet based on ensemble sensitive experiments in GFDL AM2.1.

Persad et al. (2017), based on GFDL AM3, have shown that surface solar dimming dominates the reduction of the East Asian summer precipitation due to the decreased land-sea contrast, whilst atmospheric heating from absorbing aerosols partially offset the reduction, which leads to a smaller reduction when both effects are considered simultaneously. Jiang et al. (2013) and Guo et al. (2013) indicated that there was no statistically significant change in precipitation over East China in response to global BC forcing during summertime, based on the CAM5 and HiGAM AGCM experiments, respectively. Although there are many differences across studies, some similarities can still be found in most of studies, such as surface cooling in the perturbation area, wet response in North China.

In additionSimilarly, the South Asian summer monsoon (SASM) exhibits inconsistent responses to BC forcings. some Some AGCM/CGCMmodel studies suggested that increased BC aerosols can lead to a weakened South Asian summer monsoon (SASM) (Lau and Kim, 2007; Meehl et al., 2008), while others found that there should be a strengthened SASM via increasing the atmospheric meridional land-sea thermal gradient, or an elevated heat pump effect (Lau and Kim et al., 2006; Xie et al., 2020; Westervelt et al., 2020). On the other hand, Westervelt et al. (2018) conducted aerosol removal experiments using three CGCMs, and found that Indian BC decreases lead to no change or a small decrease in precipitation in India.

In addition, Jiang et al. (2017) found that BC forcing can lead to an intensification of the East Asian winter monsoon (EAWM) northern mode via heating Tibetan Plateau using the CAM5 model. On the contrary, Lou et al. (2019) suggested that BC emitted from the North China can weaken the EAWM through ocean, sea ice, and cloud feedbacks based on CESM. BC aerosol can also affect spring and autumn precipitation in China (Guo et al., 2013; Hu and Liu, 2014; Deng et al., 2014).

135   By comparing the sum of Asian ~~summer~~ climate responses to individual responses

136   over East and South Asia with the responses to simultaneous forcing, the regional

137   linearity of BC forcing has been investigated, but the results remain unclear. Chen et al.

138   (2020) and Herbert et al. (2022) suggested that the responses were highly nonlinear due

139   to ~~the~~ interactions of atmospheric circulation changes, based on a regional climate

140   model and an atmospheric general circulation model~~the regional climate model~~

141   ~~RegCM4 and the Intermediate General Circulation Model 4 (IGCM4)~~ (AGCM),

142   respectively~~simulations, respectively~~. In contrast, Reccia and Lucarini (2023) and

143   Stjern et al. (2024) found that the responses were almost linear in most of Asian regions.

144   The difference may be related to the different spatial ~~extend~~ extent of the aerosol

145   perturbation in the simulation design (Stjern et al., 2024).

146   ~~For the East Asian winter climate, Jiang et al. (2017) found that BC forcing can~~

147   ~~lead to an intensification of the East Asian winter monsoon (EAWM) northern mode~~

148   ~~via heating Tibetan Plateau using the CAM5 model. On the contrary, Lou et al. (2019)~~

149   ~~suggested that BC emitted from the North China can weaken the EAWM through ocean,~~

150   ~~sea ice, cloud feedbacks based on CESM. BC aerosol also can impact on spring and~~

151   ~~autumn precipitation in China (Guo et al., 2013; Hu and Liu et al., 2014; Deng et al.,~~

152   ~~2014).~~

153   These inconsistent results, and the large uncertainty in the simulated response of

154   the Asian climate to BC changes, are partly related to differences in the modeling

155   approach (e.g., AGCMs versus CGCMs/ESMs) and also the magnitude and location of

156   the BC perturbation. Atmosphere-only GCMs lack SST feedbacks, which are crucial in

157   influencing the Asian monsoon (Dong et al., 2019), while CGCMs or ESMs involving

158   more and more complex physical processes make it difficult to identify the key physical

159   processes ~~of~~ behind impacts of regional BC aerosols on Asian climate. The

160   inconsistency may also be associated with model-specific differences. Different models

161   that include different physical processes, combined with different experiment designs

162   that can influence the atmospheric circulation response, ~~mean that~~make it challenging

163   to understand~~ing~~ the causes of differences between studies ~~is very difficult~~.

164   Hence, reduced complexity models, such as FORTE2 (Fast Ocean Rapid

Troposphere Experiment version 2), provide an alternative and useful tool for such studies, given that such models not only include all the main mechanisms of aerosol-climate interactions, but also allow fast speed of integration and longer simulations with lower cost. Stjern et al. (2024) have utilized FORTE2 to perform a series of Systematic Regional Aerosol Perturbations (SyRAP) simulations, employing regionally realistic aerosol forcing for the period 2003-2021 from the Copernicus Atmosphere Monitoring Service (CAMS) reanalysis (Inness et al., 2019). The core simulations with include: (1) baseline simulations forced by GHG concentrations at different climate states (i.e. pre-industrial, present-day and future CO_2 levels) and no aerosol; (2) perturbation simulations forced by added absorbing aerosols (BC, and organic carbon, OC) or scattering aerosols (sulfate, SO_4) over East Asia only, South Asia only, and over both regions simultaneously with only ARI effects, and GHG concentrations at different climate states; (3) Aerosol-cloud interactions (ACI) simulations forced by added SO_4 in the combined East Asia and South Asia region in which ACI were turned on.absorbing and scattering aerosol species in East Asia only, South Asia only, and both regions simultaneously. Their results have shown thatThe SyRAP-FORTE2 is a helpful framework enables comprehensive analysis to understand and decompose the local and remote of climate effects of different regional aerosol emissionsperturbations and aerosol species, as well as ARI versus ACI, and allows comparison of their relative importance and interactions (Stjern et al., 2024).

Therefore In this study, considering that BC aerosols mostly impact climate through ARIbased on the simulations of the regional BC perturbations in SyRAP-FORTE2, this studywe aimsaim to address the following two questions focused on BC ARI effects, based on the simulations of the regional BC perturbations in SyRAP-FORTE2: (1) what are the responses of Asian climate to either East Asian BC perturbations, or South Asian BC perturbationsemissions, or both regions simultaneouslyat once, respectively? (2) What are the key physical processes involved in these responses?

The rest of the paper is organized as follows: section 2 describes the FORTE2 model, the SyRAP simulations, and the analysis methods and datasets; section 3 briefly

195 evaluates the climatology of SyRAP simulations, examines responses to the regional

196 BC perturbations in SyRAP-FORTE2, and investigates the underlying physical

197 processes involved in these responses; section 4 compares the results of the atmospheric

198 energy budget in SyRAP-FORTE2 with those in the PDRMIP models; Finally, the

199 summary and discussion are provided in section 5.

2. Methods

2.1 The FORTE2 model

202 FORTE2 is an intermediate-complexity coupled atmosphere-ocean general

203 circulation model (Blaker et al., 2021). The atmospheric component is the Intermediate

204 General Circulation Model 4 (IGCM4) with a horizontal resolution of approximately

205 2.8° (T42), and 35 sigma levels extending up to 0.1 hPa (Joshi et al., 2015). IGCM4

206 includes schemes for radiation, land-surface properties, convection, precipitation, and

207 clouds (Zhong and Haigh, 1995; Betts and Miller, 1993). The oceanic component is the

208 Modular Ocean Model-Array (MOMA) with a horizontal grid spacing 2°×2°, and 15 z-

209 layer levels increasing in thickness with depth from 30 m at the surface to 800 m at the

210 bottom (Webb, 1996). Sea ice is represented by a barrier to heat fluxes between the

211 ocean and atmosphere components. FORTE2 runs without flux adjustments (Blaker et

212 al., 2021). Blaker et al. (2021) have thoroughly evaluated the skill of FORTE2's skill

213 in simulating the atmosphere, ocean and major climatic modes, suggesting that

214 FORTE2 can satisfactorily simulate a climate state and climate variability. Hence, given

215 the advantages of FORTE2 in terms of running speed, flexibility and economy, it is a

216 useful tool to study a wide range of climate questions. For the SyRAP-FORTE2

217 simulations, FORTE2 was updated to include a parameterization of aerosol-cloud

218 interactions, where cloud droplet effective radius in low- and mid-level clouds is

219 reduced from 15μm to 10μm in regions where optical depth is greater than 0.07.

220 However, this parameterization is only applied for scattering aerosol, and is not used in

221 the BC experiments described in the following section. The semi-direct effect of BC is

222 included.

2.2 The Regional BC perturbation simulations in SyRAP-FORTE2 simulations

~~Stjern et al. (2024) performed a set of SyRAP experiments using the FORTE2 model. The main simulations include: (1) baseline simulations forced by GHG concentrations at different climate states (i.e. preindustrial, present-day and future CO_2 levels) and no aerosol; (2) perturbation simulations forced by added absorbing (BC, and organic carbon, OC) or scattering (sulfate, SO_4) aerosols over East Asia only, South Asia only, and over both regions simultaneously with only aerosol-radiation interactions (ARI), and GHG concentrations at different climate states; (3) Aerosol-cloud interactions (ACI) simulations forced by added SO_4 in the combined East Asia and South Asia region in which the ACI were turned on. This study focusses on the effects of adding regional BC perturbations, but the SyRAP-FORTE2 design allows the impacts of different aerosol species to be compared in a consistent framework.~~

~~FORTE2 did not use aerosol gas emissions/concentrations as most CMIP6 models use.~~ SyRAP ~~Instead,~~FORTE2 used the global gridded monthly aerosol optical depths (AOD) and vertical distributions ~~were used~~ from the CAMS~~Copernicus Atmosphere Monitoring Service~~ reanalysis (CAMSRA) ~~(CAMSRA) during~~for 2003-2021 (Inness et al., 2019), rather than aerosol gas emissions/concentrations employed by most CMIP6 models. The CAMSRA incorporates anthropogenic BC emissions from the MACCity inventory (Granier et al., 2011) for 2003-2010, transitioning to Representative Concentration Pathway 8.5 emissions (Riahi et al., 2011) post-2010. The simulations were idealized with monthly AOD climatologies prescribed as repeating annual cycles. The regional annual mean BC AOD perturbation is about 0.015 for East China, and about 0.01 for India, respectively (Fig. S1). Aerosols were distributed vertically uniformly from the second lowest model layer (σ, or $p/p_{surface}$ = 0.88 or approximately 950 m above the surface) up to a pressure level p_{min}. For each gridbox, p_{min} was derived from CAMSRA as either 850 hPa or the lowest pressure level where the 2003-2021 mean BC+OC+SO_4 mixing ratio falls below 5×10^9 kg/kg, whichever value is lower. In topographic regions, additional constraints require $\sigma_{min} <$ 0.75 and $p_{min} >$ 300 hPa. The seasonal changes of the regional mean p_{min} over China and India are illustrated in Figure S2. Aerosols are not transported in FORTE2. The application of aerosol distributions from a reanalysis means that the simulations include

254   a realistic aerosol spatial distribution, but the lack of aerosol transport means that there

255   are no feedbacks between the climate response and the aerosol distribution (e.g.

256   increased precipitation leading to increased aerosol removal). For more details on

257   aerosols implementation in FORTE2, see Stjern et al. (2024).All simulations were run

258   for 200 years, with years 51-200 used for analysis.

259   There is no significant difference in Asian climate responses to BC aerosols

260   between the pre-industrial and present-day climate conditions in the SyRAP-FORTE2

261   simulations (Stjern et al., 2024). Hence, iIn this study the baseline simulation (piC) and

262   the BC perturbation simulations of three different regions at the pre-industrial climate

263   conditions (280 ppmv) were performed to explore potential physical processes of Asian

264   BC aerosols influencing the local climate (Table 1). There is no significant difference

265   in Asian climate responses to BC aerosols at different background climate states in the

266   SyRAP-FORTE2 simulations (Stjern et al., 2024). The regional annual mean BC AOD

267   perturbation is about 0.015 for East China, and about 0.01 for India, respectively

268   (Figure 1a in Stjern et al., 2024). Given that BC primarily influences climate through

269   direct scattering and absorption of radiation (Bond et al., 2013), Note that only climate

270   impacts due to ARI (including the semi-direct effect of BC) were considered here.. All

271   simulations were run for 200 years, with years 51-200 used for analysis.

272   **2.3 Analysis methods and Datasets**

273   The response to a particular regional forcing is estimated by the mean difference

274   between the perturbation simulation and the baseline simulation. Statistical significance

275   of the response is assessed using a two-tailed Student's t-test.

276   The atmospheric energy budget is applied to understand the precipitation

277   responses (Muller and O'Gorman, 2011; Richardson et al., 2016; Liu et al., 2018). The

278   energy associated with precipitation can be separated into a thermodynamic component

279   with only changes in the diabatic cooling (Q), and a dynamic component with only

280   changes in the dry static energy (DSE) flux divergence (H), as shown in Eq. (1):

281      $$L_c\delta P = \delta Q + \delta H \quad (1)$$

282   where L_c is the latent heat of condensation, P is precipitation, δ denotes a perturbation.

Then,

$$\delta Q = \delta LWC - \delta SWA - \delta SH \ (2)$$

where LWC is atmospheric longwave cooling, SWA is atmospheric shortwave absorption, and SH is sensible heat flux from the surface.

δH is calculated as a residual between $L_c\delta P$ and δQ. Furthermore, H can be seen as the sum of the changes in mean (H_m) and eddy (H_{trans}) components. δH_m can be decomposed into four components associated with dynamic and thermodynamic effects on vertical and horizontal advection of DSE, as shown in Eq. (3):

$$\delta H_m = \delta H_{Dyn\_v} + \delta H_{Thermo\_v} + \delta H_{Dyn\_h} + \delta H_{Thermo\_h}$$

$$= \int \delta\overline{\omega}\frac{\partial\overline{s}}{\partial p}\frac{dp}{g} + \int \overline{\omega}\delta(\frac{\partial\overline{s}}{\partial p})\frac{dp}{g} + \int \delta\overline{u}\bullet\nabla\overline{s}\frac{dp}{g} + \int \overline{u}\bullet\delta(\nabla\overline{s})\frac{dp}{g} \ (3)$$

where ω is vertical velocity, *s* is DSE, *p* is pressure, *g* is the gravitational acceleration, *u* is horizontal wind vector, ∇ is the horizontal gradient, and an overbar indicates climatological monthly means. Therefore, H_{Dyn_v} is related to changes in vertical velocity, H_{Thermo_v} is related to changes in vertical DSE gradients, H_{Dyn_h} is related to changes in horizontal winds, and H_{Thermo_h} is related to changes in horizontal DSE gradients. δH_{trans} is calculated as a residual between δH and δH_m.

To evaluate the ~~ability~~ skill of FORTE2 to ~~represent~~ simulate ~~the~~ observed climate variables, ~~climate~~ monthly precipitation, surface temperature (Ts), and horizontal wind components were used from the NOAA-CIRES-DOE 20th Century Reanalysis V3 (20CR) on a 2° × 2° grid spanning ~~1836~~ 1806 to 2015 (Compo et al., 2011). The 20CR is only based on surface observations of synoptic pressure of NOAA's physical Sciences Laboratory. Monthly sea level pressure (SLP) data were from the Hadley Centre (HadSLP) in a horizontal resolution of 5° × 5° (Allan & Ansell, 2006).

To compare the response of FORTE2 to BC perturbations ~~to the responses~~with those ~~of~~from CMIP class models, we used the PDRMIP 10 times the modern Asian BC concentrations/emissions perturbation simulations, and ~~the~~ their corresponding baseline simulations with modern aerosol concentrations/emissions and greenhouse gases under year-2000 conditions~~with the year 2000~~, ~~based on~~from the 5 GCMs (CESM1-CAM5, GISS-E2-R, HadGEM3, MIROC, and NorESM1; Table S1). More

312 details of the PDRMIP design can be found in Myhre et al. (2017), ~~while~~ and an
313 overview of the Asian monsoon response is given in Liu et al. (2018).

3. Results

3.1 Evaluation of baseline climate in SyRAP-FORTE2

316   Blaker et al. (2021) present a detailed overview of the FORTE2 climatology. The
317 model simulates the Asian climate well, and the more focused evaluation presented by
318 Stjern et al. (2024) ~~demonstrated~~ demonstrates that FORTE2 is an appropriate tool to
319 study the ~~Asian climate~~ effects of local aerosol perturbations on Asian climate. Here,
320 for completeness, we ~~present~~ assess an overview of the skill of FORTE2 in simulating
321 the Asian climate. The seasonal evolutions of precipitation and surface temperature (Ts)
322 in East China and India, and the climatology of lower tropospheric circulation (SLP and
323 850 hPa horizontal wind) in the baseline experiment (piC) are compared with those in
324 the reanalyses from 1851 to 1896. FORTE2 reproduces the seasonality of precipitation
325 in East China reasonably well, but slightly overestimates the averaged magnitude with
326 about 1 mm/day in summer (Fig. 1a). However, the model underestimates the
327 magnitude of South Asian Summer Monsoon precipitation by approximately 4 mm/day
328 during June-September relative to the 20CR reanalysis. Dry biases in Indian summer
329 precipitation of similar magnitudes are found in many CMIP5 and CMIP6 models
330 (Sperber et al., 2013; Wilcox et al., 2020; Liu et al., 2024). Differences between
331 reanalyses and observational datasets can also have similar magnitudes (Wilcox et al.,
332 2020). Hence, we conclude that the FORTE2 representation of monsoon precipitation
333 is suitable for our study. The model performs fairly well in the seasonality of
334 temperature and the magnitudes in both regions (Fig. 1b).
335   The simulated SLPs are generally lower than ~~that~~ those in HadSLP in all four
336 seasons, especially the Siberian High in winter, the western North Pacific Subtropical
337 High (WPSH) and the Indian Low in summer (Fig. 1c-j). Compared to the reanalyses,
338 the simulated Indian Low is ~~too~~ overly strong, and its eastern fringe and the westerly
339 from the Indian Ocean extend too far east into the western North Pacific, so does the
340 Indian summer monsoon trough (Fig. 1g and h). This corresponds to the model dry bias

341 over the Indian subcontinent (Fig. 1a and ~~S1e~~S3e-f). Meanwhile, the WPSH is too weak

342 to expand sufficiently far west, corresponding to the very weak ~~easterly~~ easterlies along

343 the southern fringe of the WPSH, which leads to relatively less rainfall over the

344 Philippines (Fig. ~~S1e~~S3e-f) and underestimates ~~of~~ the effects of the WPSH on the East

345 Asian summer monsoon (Fig. 1g-h). Despite these deficiencies, the model captures the

346 essential features of lower tropospheric circulation, precipitation and temperature over

347 Asia, which is consistent with the results of Stjern et al. (2024).

348 **3.2 Temperature and Precipitation responses**

349   Figure 2 shows spatial patterns of Ts responses to increased Asian BC aerosols in

350 four seasons. First~~ly~~, there is a substantial land cooling over the perturbed regions in all

351 four seasons, but with distinct seasonal differences in distributions and values. Under

352 BC_CHI, a cooling ~~can be seen~~is observed in most of China in winter and spring (Fig.

353 2a-b), with the area-averaged values of -0.9±1.2 K (mean value ± 1 standard deviation)

354 and -1.1±0.9 K, respectively (Fig. 3a). The large standard deviations indicate the large

355 spread of distributions of responses (Fig. ~~S2~~S4). There is a slight warming of sea surface

356 temperatures near China in spring. In summer and autumn, a cooling is seen mainly in

357 the region to the north of the Yangtze River valley, especially in North China, while

358 there is a weak warming to the south (Fig. 2c-d). The area-averaged values are therefore

359 ~~are~~ relatively smaller than those in winter and spring, ~~showing about~~with values of

360 approximately -0.7±0.7 K for summer and autumn (Fig. 3a).

361   Under BC_IND, the strongest cooling occurs in the whole India in spring with the

362 area-averaged value of -1.4±1.4 K, but with a weak warming in the tropical Indian

363 Ocean (Fig. 2f and 3b). The significant cooling is concentrated in northern India in the

364 other three seasons, with the area-averaged Ts decreased by 0.9±1.3 K for winter and

365 autumn, and 0.6±1.1 K for summer (Fig. 2e, g, h and 3b). The ocean surrounding the

366 Indian subcontinent shows a smaller cooling in the three seasons.

367   Secondly, the BC perturbations not only cause the local responses, but also non-

368 local responses through atmospheric circulations. The increased BC over East China

369 leads to a dipolar pattern in India with a warming to the north and a cooling to the south

in summer and autumn, and a significant warming in Central Asia in summer and Southeast Asia in autumn (Fig. 2c-d). BC emissions over India can induce a cooling in Southeast Asia in all seasons, with ~~and in summer the responses are~~ the strongest responses occurring in summer (~~with~~ the averaged value of about 1.15 K). Meanwhile, there is a significant cooling in central and southern China in summer and autumn, with temperature decreases of 0.3±0.7 K and 0.2±0.7 K, respectively (Fig. 2g-h and 3a). These added~~se added~~ impacts lead to a stronger~~n~~ East Asian cooling response under BC_CHI+IND than ~~that is stronger than that~~ under BC_CHI in summer and autumn (Fig. 2k-l and 3a). Moreover, comparison between the combined regional responses and the sum of individual regional responses shows nearly insignificant differences~~by comparing the responses to both regions at once to the sum of responses to the two separate regions, it is found that the differences are almost insignificant~~, suggesting that the impact of Asian BC aerosol on the Asian Ts is ~~linear~~ regionally linear in all four seasons (Fig. ~~S3~~S5).

In contrast to Ts responses, the responses in air temperature (Ta) at 850 hPa show a significant warming over much of the perturbed regions (Fig. 3c-d and 4). A cooling occurs over a few perturbed regions, such as central China under BC_CHI and BC_CHI+IND in winter (Fig. 4a, i). The vertical distribution of the temperature response is characterized by cooling at the surface and warming in the lower troposphere. This is a result of atmospheric absorption of solar shortwave radiation (SW) by BC aerosols, and is consistent with many previous studies (e.g., Li et al., 2016). Outside the perturbed regions, the Ta responses are in line with the Ts response, for example a cooling over China and Southeast Asia under BC_IND in summer and autumn (Fig. 3c and 4g, h).

Increased BC over East China primarily induces robust drying over most of China in all four seasons (Fig. 3e and 5a-d). Specifically, the spatial distribution in summer shows a substantial decrease over southern China (up to 40%), a relatively weaker decrease over north China and a weak increase over northwest China, with the area-averaged precipitation decreased by 0.5±0.5 mm/day (Fig. 3e, 5c and ~~S4c~~S6c). In spring and autumn, the decreased precipitation is mainly located in south and northeast China

400 by up to about 40% (Fig. 5b and d). Although the absolute change is the weakest in

401 winter (-0.2±0.3 mm/day), the relative change in central China decreases by up to about

402 60% (Fig. 3e, 5a and ~~S4a~~S6a). Under BC_IND, the response over the Indian

403 subcontinent is only statistically significant in summer, with a decrease of 0.5±1.1

404 mm/day (~21%) (Fig. 3f and 5g).

405 Additionally, under BC_CHI there is increased rainfall over India in summer and

406 autumn, which can counteract the local decrease due to the Indian BC forcing (Fig. 3f

407 and 5c-d). Hence, when considering the simultaneous BC forcing in the two regions

408 (BC_CHI+IND) in summer and autumn, there is no significant change in the regional

409 mean, showing a dipolar pattern with more rainfall over northern India and less rainfall

410 over southern India (Fig. 3f and 5k-l). On the other hand, BC_IND can induce a

411 significant precipitation increase over China and Southeast Asia in spring and summer

412 (Fig. 5f-g), ~~and~~ parti**ally**~~ly~~ offsett**ing** the decrease in response to BC_CHI over China.

413 Hence, the responses under BC_CHI+IND are weaker for China than those under

414 BC_CHI~~there are weaker responses under BC_CHI+IND for China than those under~~

415 ~~BC_CHI~~ (Fig. 3e). For regional linearity, the responses are almost linear (Fig. ~~S5~~S7).

416 Only a few regions exhibit nonlinear response**s**, such as a decrease over south Thailand

417 in winter and~~,~~ an increase over northeast India in spring and summer. The above

418 analysis regarding the summer part has been ~~included~~ presented in Stjern et al. (2024),

419 but is included here as a precursor to the detailed mechanistic analysis that follows.

3.3 Energy balance response

421 The following analysis mainly focuses on summer for clarity; the results ~~in~~ for the

422 other three seasons are in the supplement (Figures ~~S7~~S9-S1~~0~~2, ~~S12~~S14-~~S16~~S18). The

423 spatial patterns of net TOA and surface energy responses to regional BC aerosols in

424 summer are illustrated in figure 6. As expected, there are increases in net downward

425 TOA shortwave (SW)~~,~~ with area mean responses of 7.3~9.6 W/m^2 associated with

426 decreases in convective clouds over the perturbed regions (Fig. 6a-c and ~~S6j~~S8j-l).

427 Decreases in net surface downward SW can be seen with area mean responses of -

428 22.6~-27.8 W/m^2 due to SW absorption by BC aerosols (Fig. 6d-f). Significant

increases in low and middle clouds also contribute to the reduc~~tion in~~ed surface SW (Fig. ~~S6d~~S8d-i). Hence, there is warming in the troposphere ~~and~~ while cooling at surface in these perturbed regions. The enhanced net surface upward longwave (LW) has a small contribution to the local surface cooling with area mean responses from -3.2 to -5.8 W/m^2 (Fig. 6g-i), which is related to the ~~decreases~~ decreased ~~in~~ convective clouds (Fig. ~~S6j~~S8j-l). On the contrary, the positive changes in downward sensible heat (SH) (8.1~9.8 W/m^2) and latent heat (LH) (9.5~12.9 W/m^2) cause a warming effect partly offsetting the cooling in the perturbation regions (Fig. 6j-o). The ~~decreased~~ reduced SH is caused by the weakened vertical temperature differences between the surface and lower atmosphere~~., and t~~The decrease in ~~decreased~~ upward LH is ~~associated with~~associated with upper-level heating ~~aloft~~through atmospheric stabilization that suppresses moisture transport, and reduced soil moisture availability due to decreased rainfall~~and precipitation~~. Outside the perturbation regions, the negative changes in SW, LW and LH are responsible for the cooling in Southeast Asia and south China induced by the increased BC in India (Fig. 6e, h, n). Similar results can be seen in other three seasons (Table S2).

Figure 7 shows area-averaged atmospheric column energy budget terms (see Eq. 1) over East China and India in summer. For the drying in East China/India under BC_CHI/BC_IND, the substantial reductions of the diabatic cooling (δQ) are the prime driver of the decreases in the energy of precipitation (L$_c$$\delta$P), while the increases in the DSE flux divergence (δH) offset the effect of δQ to a large extent.

The enhanced precipitation in China under BC_IND, and in India under BC_CHI, is the result of increased δH (blue and green bars in Fig. 7 are almost identical), with negligible contribution from δQ. Hence, the local precipitation response to local BC increases is largely driven by δQ, while the remote precipitation response is largely driven by δH. Consequently, it can be found that the larger changes in δH lead to the smaller responses in L$_c$$\delta$P over China and India under BC_CHI+IND, relative to the changes under BC_CHI and BC_IND. It should be mentioned that the relatively large uncertainties (error bars in Fig. 7) of L$_c$$\delta$P mainly depend on δH. The other three seasons show the similar results (Fig. ~~S7~~S9).

459 Spatially, δQ shows a significant decrease throughout the entire perturbed regions

460 in the three simulations, with large decreases located over North China and northern

461 India (Fig. 8d-f). Under BC_CHI, δH ~~is characterized by~~exhibits a dipolar pattern with

462 positive changes in north of the Yangtze River and negative in south (Fig. 8g). Hence,

463 δH and δQ cancel each other out in North and Northeast China, ~~and~~ while combine with

464 each other in south of the Yangtze River. As a result, there is the strongest precipitation

465 decrease ~~in precipitation~~ in south China, and a relatively weaker decrease in north China

466 (Fig. 8a). Under BC_IND, significant positive ~~changes in~~ δH can be found along the

467 southern edge of Himalayas and the southern tip of the Indian subcontinent, and weak

468 and nonsignificant negative changes in central India (Fig. 8h). δH can therefore offset

469 the negative changes in δQ in north and south India. The substantial L_cδP reduction ~~is~~

470 ~~concentrated~~ in central India is mainly ~~due to~~driven by δQ (Fig. 8b).

471 In addition, δH is the dominating factor for L_cδP beyond the perturbation regions,

472 for example positive changes in northeast India under BC_CHI~~,~~ and ~~positive changes~~

473 from Southeast Asia to the tropical western Pacific and central China under BC_IND

474 (Fig. 8g-h). Under BC_CHI+IND, ~~it can be found that~~ the extent and magnitude of δH

475 are larger than those in the simulations of individual regions (Fig. 8i), which indicates

476 ~~more~~ greater balance between δH and δQ, corresponding to relatively weaker

477 precipitation over East China and India (Fig. 7 and 8c). Relative to summer, δQ and δH

478 ~~has~~ have negative and positive changes, respectively, ~~in the whole~~throughout the

479 perturbation regions in the other three seasons~~, respectively~~ (Fig. ~~S8~~S10-12~~0~~). In winter

480 and spring, there is a marked seesaw pattern of δH between Asia and the tropical Indian

481 Ocean and maritime continent under BC_CHI+IND, ~~leading to less~~reducing

482 precipitation in the latter regions (Fig. ~~S8c~~S10c, i and ~~S9c~~S11c, i). Overall, the

483 combined effect of δH and δQ shape the spatial pattern of precipitation responses to the

484 regional BC.

485 The reductions in δQ (see Eq. 2) are dominated by the strong atmospheric heating

486 due to SW absorption by BC aerosols (−δSWA), and also contributed by the small

487 decreases in the atmospheric longwave cooling (δLWC) (Fig. ~~S11a~~S13a-f). The sensible

488 heat flux from the surface (−δSH) ~~plays a role in~~slightly increas~~ing~~es

489   δQ~~, but with relatively small values~~ (Fig. ~~S11g~~S13g-i).

3.4 Dynamic processes responsible for responses

490   Due to storage constraints, 3D atmospheric output from FORTE2 was archived on
491   three pressure levels, 250 hPa, 500 hPa, and 850hPa, to capture ~~three~~ key aspects of the
492   tropospheric circulation response. While this precludes ~~a~~ quantitative analysis of the
493   component terms ~~of~~ of H_m and H_{trans}~~δH_m (Eq. 3)~~, it is sufficient to identify the ~~to~~ main
494   contribut~~ing term~~or to H_m. We now examine the four terms of δH_m (see Eq. 3),
495   including the dynamic components with changes in vertical and horizontal atmospheric
496   circulations (δH_{Dyn_v} and δH_{Dyn_h}), and thermodynamic components with changes in
497   vertical and horizontal DSE gradients (δH_{Thermo_v} and δH_{Thermo_h}). Figure 9 displays
498   spatial patterns of the four components in summer in the three simulations. In general,
499   the δH_{Dyn_v} highly resembles the δH in ~~the three~~all simulations, and the magnitudes in
500   δH_{Dyn_v} are far greater than those in the other three terms, suggesting that dynamic
501   effect of vertical circulation is the primary contributor to δH (Fig. 9a-c). δH_{Thermo_v}
502   and δH_{Dyn_h} ~~are small~~show minimal anomalies in all regions for all experiments.
503   Larger anomalies are seen in δH_{Thermo_h}, where negative anomalies offset some of the
504   influence of δH_{Dyn_v} over the Indo-China peninsula in the BC_IND and BC_CHI+IND
505   experiments. However, these anomalies are ~~not~~ insufficient to influence the sign of δH,
506   which is still primarily driven by δH_{Dyn_v} in this region. In the other seasons, δH_{Dyn_v}
507   remains the most important factor (Fig. ~~S12~~S14-~~14~~16), although it is more strongly
508   offset by δH_{Dyn_h} and δH_{Thermo_h} in winter. The effects of horizontal circulation are
509   relatively weak in spring and autumn.

510   Based on the above analysis, we conclude that vertical movement is the ~~most~~
511   ~~important~~primary contributor to δH_m. As expected, the spatial patterns of responses in
512   ~~Omega (~~vertical velocity (Omega)~~)~~ at 500 hPa correspond well to those in δH_{Dyn_v} (Fig.
513   10a-c). Anomalous ascent corresponds to the increase in δH_{Dyn_v}, leading to more

515 precipitation, which offsets the precipitation reduction driven by decreased δQ. While

516 aAnomalous descent amplifies suppresses precipitation suppression, adding to the

517 precipitation reduction driven caused by the reducetion ind δQ.

518   Why does the vertical velocity exhibit such changes? It seems to be related to the

519 tropospheric —temperature responses in the troposphere, reflected by a good

520 corresponding relationship between the Omega and Ta responses at 500 hPa (Fig. 10a-

521 f). The warm anomalies favor a divergence in the middle troposphere, which in turn are

522 associated with anomalous ascent. The cold anomalies are associated with a

523 convergence and descending motion. The above-mentioned relationship also exists in

524 the other seasons, and it is more pronounced at 850 hPa (Fig. 4 and S15S17).

525   From the transects of zonal mean diabatic heating over the perturbation regions,

526 changes to tropospheric heating can be seen more clearly (Fig. 11). Under BC_CHI, the

527 responses in diabatic heating show a meridional dipolar structure through the whole

528 troposphere over East China, with a cooling over the region to south of 32°N (the

529 Yangtze River basin), and a warming to north (Fig. 11a). The dipolar pattern

530 corresponds well to the meridional distributions of precipitation, vertical velocity and

531 Ta at 500 hPa. The cooling center located at the middle troposphere is due to the reduced

532 latent heat release caused by the substantial decrease in precipitation over south China.

533 The heating center at the lower troposphere in the north mainly results from SW

534 absorption by increased BC aerosol. The difference between south China and north

535 China is associated with the larger AOD perturbation imposed north of the Yangtze

536 basin in SyRAP-FORTE2 (Stjern et al., 2024Fig. S1). In BC_CHI+IND, there is a

537 similar dipolar pattern, except for a warming at the lower troposphere around south of

538 30°N (Fig. 11b). The warming is related to the increased precipitation over south China

539 because of the BC aerosols over India.

540   For India in BC_IND, there is also a cooling center associated with the reduced

541 precipitation in the middle troposphere (Fig. 11c), corresponding to a cold anomaly and

542 descending motion at 500 hPa (Fig. 10b, e). In the lower troposphere, a warming can

543 be seen at south of the Qinghai-Tibet Plateau. Compared with BC_IND, the cold

544 anomaly is weaker, but the warm anomalies are strengthened under BC_CHI+IND (Fig.

11d). Hence, a significant ascending motion can be found in northeast India resulted from the effect of increased BC over East Asia (Fig. 10c), which is consistent with that in Herbert et al. (2022). In the other three seasons, however, unlike in summer, there is no cooling center in the middle troposphere, and the heating centers are situated at the lower troposphere (Fig. S16S18). Overall, the diabatic heating induced by the increased BC aerosols at the lower troposphere leads to an ascending motion explaining the increased δH over the perturbation regions.

Considering that the dynamic and thermodynamic effects of horizontal atmospheric circulations have some contributions to δH, we look at the changes in lower tropospheric horizontal circulation in response to changes of regional BC aerosols (Fig. 10g-i). Under BC_CHI, the cyclone anomaly over East China leads to anomalous easterly wind over North China with cutting off the moisture supply from south (Fig. 10g). Under BC_IND, the westerly anomalies associated with the cyclonic circulation over India favor to strength the Indian summer monsoon, which corresponds to the increase in δH_{Dyn_h} (Fig. 10h). The responses in the circulations to both regions at once can be seen as the sum of responses to the two separate regions (Fig. 10i). Additionally, there is a cyclonic circulation over East China and an anticyclonic circulation over central China in winter under BC_CHI (Fig. S17S19), leading to anomalous northerly wind across central China and then suppress precipitation over there, which is in agreement with the decrease in δH_{Dyn_h} (Fig. S10gS14g). The changes in horizontal circulations are related to the changes in Ta and omega in the lower troposphere (Fig. 4 and S15S17).

4   Energy budget analysis in other coupled models

To evaluate the precipitation response and the mechanisms in FORTE2, we compare the results of energy budget analysis (see Eq. 1) in the PDRMIP simulations forced by 10 times the present-day Asian BC concentrations/emissions in five CMIP-class models to those in the SyRAP-FORTE2 BC_CHI+IND experiment. Spatial patterns of summer energy budgets in the PDRMIP and FORTE2 models are illustrated

573   in Figure 12. There are significant decreases in δQ over most of Asia in all of the

574   PDRMIP models, which is generally consistent with the results under BC_CHI+IND

575   (Fig. ~~12f~~12g-~~j~~l). Three models (CESM1-CAM5, GISS-E2-R and NorESM1) have

576   similar distributions of δQ to BC_CHI+IND, showing a maximum center in North

577   China and northern India.~~-~~ δH increases significantly in India and most of East China

578   in these models (Fig. ~~12k~~12m, ~~l~~n, ~~o~~q), again roughly resembling the changes of

579   BC_CHI+IND (Fig. ~~8i~~12r), while the other two models show a significant increase in

580   north~~ern~~ India and North China with weaker magnitudes (Fig. ~~12m~~12o-~~n~~p). The

581   PDRMIP multi-model mean changes in δH [figure 7 in Liu et al. (2018)] are also

582   similar to the changes in BC_CHI+IND. In addition, GISS-E2-R and MIROC show

583   evident decreases in δH and precipitation in Southeast Asia, while the other three

584   models show no significant changes. This is contrary to the significant increases seen

585   in FORTE2. There are large differences in the total L_cδP responses across these models

586   (Fig. 12a-f). However, some precipitation changes are consistent in most of the models,

587   such as decreases over South China and increases over North China and northern

588   India.~~In spite of these model differences in the individual terms, models are broadly~~

589   ~~consistent in their total L_cδP responses. Precipitation generally increases over India and~~

590   ~~North China, and decrease over South China in the PDRMIP models and FORTE2 (Fig.~~

591   ~~12a-e). There is no significant increase in δH and precipitation in Southeast Asia in the~~

592   ~~PDRMIP models.~~

593   Figure 13 shows the regional means of each energy budget term over East China

594   and India in summer under the PDRMIP and FORTE2 models. There is a weak and

595   insignificant reduction in L_cδP from -0.6 (HadGEM3) to -7.2 W/m^2 (NorESM1) for

596   East China, which ~~are~~ is comparable to the value of -3.8 W/m^2 under BC_CHI+IND

597   (Fig. 13a). Hence, ~~the result under BC_CHI+IND in FORTE2 is agreement with the~~

598   ~~PDRMIP models, suggesting that~~ the increased BC perturbations over Asia lead to

599   slight decreases in precipitation over East China in all of the models. The regional

600   means range from -1.2 (MIROC) to 13.7 W/m^2 (NorESM1) for India (Fig. 13b). Except

601   for MIROC, L_cδP in the other models have stronger increases than that under

602   BC_CHI+IND, about 0.6 W/m^2, which may be related to the larger drying bias of Indian

603 summer precipitation in FORTE2, or the much larger BC perturbation in PDRMIP.

604   The effect of δQ decreases $L_c \delta P$ with a large range from -4.7 (HadGEM3) to -29.8

605 W/m^2 (GISS-E2-R) for East China, while δH has an opposite effect from 2.1 (MIROC)

606 to 24.4 W/m^2 (GISS-E2-R) (Fig. 13a). Similarly, δQ changes from -5.7 (HadGEM3) to

607 -25.8 W/m^2 (GISS-E2-R) for India, and δH from 4.9 (MIROC) to 36.5 W/m^2 (GISS-

608 E2-R) (Fig. 13b). The magnitudes in δQ and δH under the PDRMIP models are much

609 smaller than those in FORTE2 in both ~~the two~~ regions, except for GISS-E2-R. The

610 negative effect of δQ and the positive effect of δH ~~also~~ can also be seen in the PDRMIP

611 multimodel mean for the whole Asian region (Liu et al., 2018). There are ~~Despite~~

612 ~~large~~substantial differences in the magnitudes and spatial patterns of their responses,

613 which are to be expected from their large range of aerosol radiative forcing and

614 climatological precipitation. However, these precipitation responses among, ~~the results~~

615 ~~of~~ these models are overall consistent qualitatively, indicating that thermodynamic

616 processes dominantly decrease precipitation, while dynamic processes increase

617 precipitation and partially offset the effects of δQ.

5   Conclusion and Discussion

619   In this study, we have investigated the Asian climatic responses to adding BC

620 aerosols to the separate regions (East China and India), and both regions at once, and

621 examined the associated physical processes, with the SyRAP simulations based on the

622 reduced-complexity climate model FORTE2. Our main findings are as follows.

623   i.   BC increases over East Asia or South Asia lead to a local strong surface cooling

624 and lower tropospheric air temperature warming in all four seasons, with seasonal

625 differences in magnitude and spatial distribution. The responses in temperature are

626 dominated by the substantial decreases in surface SW radiation due to SW absorption

627 by BC aerosols. BC over East Asia causes significant drying in south and northeast

628 China in spring, summer and autumn. In winter, there is a significant reduction in

629 central China. BC over South Asia induces a substantial decrease in rainfall in India in

630 summer. Also, South Asian BC induces significant ~~decreases in~~ temperature decreases

631 and precipitation increases in Southeast Asia ~~in~~ during summer and autumn.

632 ii.   Responses in temperature and precipitation to Asian BC forcing are mostly

633 linear regionally in all four seasons. There are relatively smaller decreases in

634 precipitation responses to adding BC over both regions simultaneously, compared to

635 the local reductions in precipitation responses to BC increases over East Asia and South

636 Asia separately. This is because BC over East Asia (BC over India) increases

637 precipitation in northeastern India, while BC over South Asia increases precipitation

638 over southern and central China.

639 iii.   Using an energy budget analysis, we find that reductions in the energy of local

640 precipitation ($L_c\delta P$) over the perturbation regions result from decreases in net

641 atmospheric diabatic cooling (δQ). The increases in the dry static energy (DSE) flux

642 divergence (δH) play a role in offsetting the effects of δQ to a large extent.

643 Consequently, the responses in precipitation to Asian BC can be considered as the result

644 of interactions between thermodynamic and dynamic processes. For δQ, the reductions

645 are mainly due to the strong atmospheric heating ($-\delta SWA$). For δH, the increases

646 depend mainly on the positive changes in the dynamic processes associated with

647 vertical atmospheric circulations (δH_{Dyn_v}). We find that δH_{Dyn_v} patterns correspond

648 well to vertical velocity change patterns at the middle and lower troposphere.

649 Anomalous ascent is primarily triggered by the warming in the middle and lower

650 troposphere over north China in summer and in most of Asia in the other seasons.

651 However, there is anomalous descent in southern China and central India in summer,

652 which is a result of cool anomalies in the middle troposphere due to the reduced latent

653 heat release caused by the substantial decrease in precipitation. The difference in

654 diabatic heating at the middle and lower troposphere is related to the difference in

655 spatial distributions of AOD in the different seasons.

656   It is well known that the EASM and SASM underwent weakening trends during

657 the second half of the 20th century (Wang et al., 2001; Bollasina et al., 2011). Although

658 the variations of ASM have been attributed to many factors including internal

659 variability and external forcing, the strong increases in BC emissions from East and

660 South Asia (Lund et al., 2019) could play a role in weakening the ASM over the past

661 decades according to this study. The increased BC ~~also~~ could also alleviate the enhanced

662 precipitation over south China due to GHG increase since the mid-1990s (Tian et al.,

663 2018). Since the early 2010s, anthropogenic aerosols (including BC and sulfate) have

664 been decreasing in East China, while they have continued to rise in India; these are

665 trends which are expected to continue over the coming decades (Lund et al., 2019;

666 Samset et al., 2019). Hence, there is a new dipole pattern characterized by decreasing

667 aerosols over East China and increasing aerosols over India. Given that responses to

668 Asian BC forcing are linear regionally in the SyRAP-FORTE2 simulations, the impacts

669 of the dipole pattern on the Asian climate can be roughly estimated by the sum of

670 responses to BC over China multiplied by -1 and responses to BC over India. The result

671 shows that there are warm anomalies in north China and cold anomalies in south China,

672 southeast Asia and most of India, and positive precipitation anomalies over most of

673 China (especially south China) and southeast Asia, and negative anomalies over India

674 (Fig. ~~S18~~S20). It is overall consistent with the result in Xiang et al. (2023), although

675 their result involves the combined effect of BC and sulfate.

676 Comparative analysis with the CGCMs/ESMs results from PDRMIP has

677 elucidated the key physical mechanisms of Asian climate responses to regional BC

678 perturbations. The thermodynamic process dominates the precipitation reduction, while

679 the dynamic process provides partial compensation. The SyRAP-FORTE2 experiment

680 series allows systematic comparison of impacts of different Asian subregions, aerosol

681 species, and climate backgrounds within a consistent modeling framework. Notably,

682 FORTE2 includes a parameterization of ACI, enabling direct comparison of the relative

683 contributions of ARI and ACI. These related works will be conducted in next step, and

684 may provide new insights into regional aerosol impacts.

685 Large differences in the magnitude and spatial pattern of precipitation responses

686 to BC ~~can be~~exist across all the models. These discrepancies may partly be due to the

687 much larger BC perturbation in PDRMIP, and partly be due to model-specific

688 differences. The FORTE2 simulation only accounts for ARI effects, incorporating the

689 semi-direct effect of BC, while PDRMIP models exhibit varying treatments of indirect

690 effects. The models with all aerosol indirect effects (particularly CESM1-CAM5 and

NorESM1) increase precipitation over India, contrasting with the reduced precipitation in FORTE2. Additionally, despite the much weaker BC forcing in FORTE2, it produces larger thermodynamic (δQ) and dynamic (δH) responses than most PDRMIP models (except for GISS-E2-R). This may arise from the absence of wet deposition feedbacks in FORTE2 (Stjern et al., 2024). ~~The smaller precipitation responses over India in FORTE2 relative to PDRMIP may partly be due to much larger BC perturbation in PDRMIP. Liu et al. (2024) have proposed that the responses of Asian summer rainfall to Asian aerosols are strongly modulated by regional precipitation biases. Some other factors or mechanisms may play a role in causing differences in responses to Asian BC, such as bias of atmospheric circulations, land-atmosphere interaction.~~ Further work to understand the mechanisms behind model differences in the response to BC would help to reduce uncertainties and ~~would~~ improve the confidence in future Asian climate change projections.

Acknowledgements. This work is supported by the Second Tibetan Plateau Scientific Expedition and Research Program (2019QZKK010203). Some of the research presented in this paper was carried out on the High Performance Computing Cluster supported by the Research and Specialist Computing Support service at the University of East Anglia. We acknowledge the Center for Advanced Study in Oslo, Norway that funded and hosted our HETCLIF centre during the academic year of 2023/24. F. L. is supported by the Scientific Research of Chengdu University of Information Technology (Grant No. KYTZ202210). B. H. S., C. W. S., L. J. W., M. J. and R. J. A were supported by the Research Council of Norway [Grant 324182 (CA3THY)].

Data availability. The NOAA-CIRES-DOE 20th Century Reanalysis V3 (20CR) datasets are obtained from https://psl.noaa.gov/data/gridded/data.20thC_ReanV3.html. The HadSLP2r is provided by the UK Met Office Hadley Centre and can be downloaded from at http://www.metoffice.gov.uk/hadobs/hadslp2/. The PDRMIP data can be accessed through the World Data Center for Climate (WDCC) data server at https://doi.org/10.26050/WDCC/PDRMIP_2012-2021. Data of the SyRAP-FORTE2 experiments reported in this paper are available without restriction on reasonable

720 request from Camilla W. Stjern at CICERO Center for International Climate Research.

721 **Author contribution.** F. L. and B. H. S. designed the study. C. W. S., L. J. W., M. J.

722 ran the model simulations. F. L. carried out the analysis and visualized the results. All

723 authors discussed the results and edited the paper.

724 **Competing interests.** L. J. W. is a member of the editorial board of *Atmospheric*

725 *Chemistry and Physics*.

726 **References**

727 Allan, R. and Ansell, T.: A new globally-complete monthly historical gridded mean sea

728   level pressure dataset (HadSLP2): 1850-2004, J. Climate, 19, 5816-5842,

729   https://doi.org/10.1175/JCLI3937.1, 2006.

730 Betts, A. K. and Miller, M. J.: The Betts-Miller scheme, in: The Representation of

731   Cumulus Convection in Numerical Models of the Atmosphere, Chapter 9, edited

732   by: Emanuel, K. A. and Raymond, D. J., Amer. Meteor. Soc., Meteor. Mon., 24,

733   107-121, 1993.

734 Blaker, A. T., Joshi, M., Sinha, B., Stevens, D. P., Smith, R. S., and Hirschi, J. J.-M.:

735   FORTE 2.0: a fast, parallel and flexible coupled climate model, Geosci. Model

736   Dev., 14, 275-293, 10.5194/gmd-14-275-2021, 2021.

737 Bollasina, M. A., Ming, Y. and Ramaswamy, V.: Anthropogenic aerosols and the

738   weakening of the South Asian summer monsoon, Science, 334, 502-505,

739   https://doi.org/10.1126/science.1204994, 2011.

740 Bond, T. C., Doherty, S. J., Fahey, D. W., Forster, P., Berntsen, T., DeAngelo, B.,

741   Flanner, M., Ghan, S., Kächer, B., Koch, D., Kinne, S., Kondo, Y., Quinn, P. K.,

742   Sarofim, M. C., Schultz, M. G., Schulz, M., Venkataraman, C., Zhang, H., Zhang,

743   S., Bellouin, N., Guttikunda, S. K., Hopke, P. K., Jacobson, M. Z., Kaiser, J. W.,

744   Klimont, Z., Lohmann, U., Schwarz, J. P., Shindell, D., Storelvmo, T., Warren, S.

745   G., and Zender, C. S.: Bounding the role of black carbon in the climate system: A

746   scientific assessment, J. Geophys. Res.-Atmos., 118, 5380-552, 2013.

747 Chen, H., Zhuang, B., Liu, J., Li, S., Wang, T., Xie, X., Xie, M., Li, M. and Zhao, M.:

Regional Climate Responses in East Asia to the Black Carbon Aerosol Direct Effects from India and China in Summer, J. Climate, 33, 9783-9800, https://doi.org/10.1175/JCLI-D-19-762 0706.1, 2020.

Compo, G. P., Whitaker, S., Sardeshmukh, J., Matsui, N., Allan, R. J., Yin, X., Gleason, B. E., Vose, R. S., Rutledge, G., Bessemoulin, P., Brönnimann, S., Brunet, M., Crouthamel, R. I., Grant, A. N., Groisman, P. Y., Jones, P. D., Kruk, M. C., Kruger, A. C., Marshall, G. J., Maugeri, M., Mok, H. Y., Nordli, Ø., Ross, T. F., Trigo, R. M., Wang, X. L., Woodruff, S. D. and Worley, S. J.: The Twentieth Century Reanalysis Project, Q. J. Roy. Meteor. Soc., 137, 1-28, 2011.

Deng, J., Xu, H., Ma, H., Jiang Z.: Numerical study of the effect of anthropogenic aerosols on spring persistent rain over eastern China, J. Meteorol. Res., 28, 341-353, 2014.

Dong, B., Wilcox, L. J., Highwood, E. J., and Sutton, R. T.: Impacts of recent decadal changes in Asian aerosols on the East Asian summer monsoon: roles of aerosol–radiation and aerosol–cloud interactions, Clim. Dyn., 53, 3235–3256, https://doi.org/10.1007/s00382-019-04698-0, 2019.

Granier, C., Bessagnet, B., Bond, T., D'Angiola, A., Denier van der Gon, H., Frost, G. J., Heil, A., Kaiser, J. W., Kinne, S., Klimont, Z., Kloster, S., Lamargue, J. F., Liousse, C., Masui, T., Meleux, F., Mieville, A., Ohara, T., Raut, J. C., Riahi, K., Schultz, M. G., Smith, S. J., Thompson, A., Aardenne, J., van der Werf, G. R., and van Vuuren, D. P.: Evolution of anthropogenic and biomass burning emissions of air pollutants at global and regionalscales during the 1980–2010 period, Climatic Change, 109, 163-190, https://doi.org/10.1007/s10584-011-0154-1, 2011.

Gu, Y., Liou, K. N., Xue, Y., Mechoso, C. R., Li, W. and Luo, Y.: Climatic effects of different aerosol types in China simulated by the UCLA general circulation model, J. Geophys. Res., 111, D15201, doi:10.1029/2005JD006312, 2006.

Guo, L., Highwood, E. J., Shaffrey, L. C. and Turner, A. G.: The effect of regional changes in anthropogenic aerosols on rainfall of the East Asian Summer Monsoon, Atmos. Chem. Phys., 13, 1521-1534, https://doi.org/10.5194/acp-13-1521-2013,

777   2013.

778   Guo, L., Turner, A. and Highwood, E.: Impacts of 20th century aerosol emissions on

779   the South Asian monsoon in the CMIP5 models, Atmos. Chem. Phys., 15, 6367-

780   6378, https://doi.org/10.5194/acp-15-6367-2015, 2015.

781   Herbert, R., Wilcox, L. J., Joshi, M., Highwood, E. and Frame, D.: Nonlinear response

782   of Asian summer monsoon precipitation to emission reductions in South and East

783   Asia, Environ. Res. Lett., 17, 014005, 10.1088/1748-9326/ac3b19, 2022.

784   Hu, N. and Liu, X.: Modeling study of the effect of anthropogenic aerosols on late

785   spring drought in South China, Acta Meteorol. Sin., 27, 701-715,

786   doi:10.1007/s13351-013-0506-z, 2014.

787   Inness, A., Ades, M., Agustí-Panareda, A., Barré, J., Benedictow, A., Blechschmidt, A.-

788   M., Dominguez, J. J., Engelen, R., Eskes, H., Flemming, J., Huijnen, V., Jones, L.,

789   Kipling, Z., Massart, S., Parrington, M., Peuch, V.-H., Razinger, M., Remy, S.,

790   Schulz, M., and Suttie, M.: The CAMS reanalysis of atmospheric composition,

791   Atmos. Chem. Phys., 19, 3515-3556, 10.5194/acp-19-3515-2019, 2019.

792   IPCC, 2021: Climate Change 2021: The Physical Science Basis. Contribution of

793   Working Group I to the Sixth Assessment Report of the Intergovernmental Panel

794   on Climate Change [Masson-Delmotte, V., P. Zhai, A. Pirani, S.L. Connors, C.

795   Péan, S. Berger, N. Caud, Y. Chen, L. Goldfarb, M.I. Gomis, M. Huang, K. Leitzell,

796   E. Lonnoy, J.B.R. Matthews, T.K. Maycock, T. Waterfield, O. Yelekçi, R. Yu, and

797   B. Zhou (eds.)]. Cambridge University Press, Cambridge, United Kingdom and

798   New York, NY, USA, 2391 pp. doi:10.1017/9781009157896.

799   Jiang, Y., Liu, X., Yang, X. Q. and Wang, M.: A numerical study of the effect of different

800   aerosol types on East Asian summer clouds and precipitation, Atmos. Environ., 70,

801   51-63, 2013.

802   Jiang, Y., Yang, X. Q., Liu, X., Yang, D., Sun, X., Wang, M., Ding, A., Wang, T. and Fu,

803   C.: Anthropogenic aerosol effects on East Asian winter monsoon: The role of black

804   carbon-induced Tibetan Plateau warming, J. Geophys. Res. Atmos., 122, 5883-

805   5902, doi:10.1002/2016JD026237, 2017.

806   Joshi, M., Stringer, M., van der Wiel, K., O'Callaghan, A. and Fueglistaler, S.: IGCM4:

807   a fast, parallel and flexible intermediate climate model, Geosci. Model Dev., 8,

808   1157-1167, 10.5194/gmd-8-1157-2015, 2015.

809   Lau, K. M., Kim, M. K. and Kim, K. M.: Asian monsoon anomalies induced by aerosol

810   direct forcing: the role of the Tibetan Plateau, Clim. Dynam., 26, 855-664, 2006.

811   Lau, K. M. and Kim, K. M.: Does aerosol strengthen or weaken the Asian monsoon? in

812   Mountains: Witnesses of Global Change, edited by: Baudo, R., Tartari, G., and

813   Vuillermoz, E., Elsevier, Amsterdam, the Netherlands, 2007.

814   Li, J., Carlson, B. E., Yung, Y. L., Lv, D., Hansen, J., Penner, J., Liao, H., Ramaswamy,

815   V., Kahn, R., Zhang, P., Dubovik, O., Ding, A., Lacis, A., Zhang, L. and Dong,

816   Y.: Scattering and absorbing aerosols in the climate system, Nat. Rev. Earth.

817   Environ., 3, 363-379, https://doi.org/10.1038/s43017-022-00296-7, 2022.

818   Li, Z., Lau, W. K., Ramanathan, V., Wu, G., Ding, Y., Manoj, M. G., Liu, J., Qian, Y.,

819   Li, J., Zhou, T., Fan, J., Rosenfeld, D., Ming, Y., Wang, Y., Huang, J., Wang, B.,

820   Xu, X., Lee, S. S., Cribb, M., Zhang, F., Yang, X., Takemura, T., Wang, K., Xia,

821   X., Yin, Y., Zhang, H., Guo, J., Zhai, P. M., Sugimoto, N., Babu, S. S., and Brasseur,

822   G. P.: Aerosol and Monsoon Climate Interactions over Asia, Rev. Geophys., 54,

823   866–929, https://doi.org/10.1002/2015rg000500, 2016.

824   Liu, L., Shawki, D., Voulgarakis, A., Kasoar, M., Samset, B. H., Myhre, G., Forster, P.

825   M., Hodnebrog, Ø, Sillmann, J., Aalbergsjø, S. G., Boucher, O., Faluvegi, G.,

826   Iversen, T., Kirkevåg, A., Lamarque, J., Olivié, D., Richardson, T., Shindell, D.

827   and Takemura, T.: A PDRMIP Multimodel Study on the Impacts of Regional

828   Aerosol Forcings on Global and Regional Precipitation, J. Climate, 31, 4429-4447,

829   https://doi.org/10.1175/JCLI-D-17-0439.1, 2018.

830   Liu, Z., Bollasina, M. and Wilcox, L.: Impact of Asian aerosols on the summer monsoon

831   strongly modulated by regional precipitation biases, EGUsphere [preprint],

832   https://doi.org/10.5194/egusphere-2023-3136, 2024.

833   Lou, S., Yang, Y., Wang, H., Lu, J., Smith, S., Liu, F. and Rasch, P.: Black Carbon

834   Increases Frequency of Extreme ENSO Events, J. Climate, 32, 8323-33,

835   https://doi.org/10.1175/JCLI-D-19-0549.1, 2019.

836   Lou, S., Yang, Y., Wang, H., Smith, S., Qian, Y. and Rasch, P.: Black carbon amplifies

837   haze over the North China Plain by weakening the East Asian winter monsoon,

838   Geophys. Res. Lett., 46, 452-460, https://doi.org/10.1029/2018GL080941, 2019.

839   Lund, M. T., Myhre, G. and Samset, B. H.: Anthropogenic aerosol forcing under the

840   Shared Socioeconomic Pathways, Atmos. Chem. Phys., 19, 13827-13839,

841   https://doi.org/10.5194/acp-19-13827-2019, 2019.

842   Mahmood, R. and Li, S.: Remote influence of South Asian black carbon aerosol on East

843   Asian summer climate, Int. J. Clim., 34, 36-48, https://doi.org/10.1002/joc.3664,

844   2014.

845   Meehl, G. A., Arblaster, J. M. and Collins, W. D.: Effects of black carbon aerosols on

846   the Indian monsoon, J. Climate, 21, 2869-2882,

847   https://doi.org/10.1175/2007JCLI1777.1, 2008.

848   Muller, C. J. and O'Gorman, P. A.: An energetic perspective on the regional response

849   of precipitation to climate change. Nat. Climate Change, 1, 266-271,

850   https://doi.org/10.1038/nclimate1169, 2011.

851   Menon, S., Hansen, J., Nazarenko, L., Nazarenko, L. and Luo, Y.: Climate effects of

852   black carbon aerosols in China and India, Science, 297, 2250-2253, 2002.

853   Myhre, G., Forster, P., Samset, B., Hodnebrog, Ø, Sillmann, J., Aalbergsjø, S. G.,

854   Andrews, T., Boucher, O., Faluvegi, G. and Flächner, D.: PDRMIP: A precipitation

855   driver and response model intercomparison project, protocol and preliminary

856   results, B. Am. Meteorol. Soc., 98, 1185-1198, https://doi.org/10.1175/BAMSD-

857   16-0019.1, 2017.

858   Persad, G. G., Paynter, D. J., Ming, Y. and Ramaswamy, V.: Competing Atmospheric

859   and Surface-Driven Impacts of Absorbing Aerosols on the East Asian Summertime

860   Climate, J. Climate, 30, 8929-49, https://doi.org/10.1175/JCLI-D-16-0860.1, 2017.

861   Ramanathan, V. and Carmichael, G.: Global and regional climate changes due to black

862   carbon, Nat. Geosci., 1, 221-227, https://doi.org/10.1038/ngeo156, 2008.

863   Recchia, L. G. and Lucarini, V.: Modelling the effect of aerosol and greenhouse gas

864   forcing on the South Asian and East Asian monsoons with an intermediate-

865   complexity climate model, Earth Syst. Dynam., 14, 697-722, 10.5194/esd-14-697-

866   2023, 2023.

Riahi, K., Rao, S., Krey, V., Cho, C., Chirkov, V., Fischer, G., Kindermann, G., Nakicenovic, N., Rafaj, P.: Rcp 8.5—A scenario of comparatively high greenhouse gas emissions, Climatic Change, 109, 33-57, https://doi.org/10.1007/s10584-011-0149-y, 2011.

Richardson, T. B., Forster, P. M., Andrews, T. and Parker, D.: Understanding the rapid precipitation response to CO2 and aerosol forcing on a regional scale. J. Climate, 29, 583-594, https://doi.org/10.1175/JCLI-D-15-0174.1, 2016.

Samset, B. H., Lund, M. T., Bollasina, M., Myhre, G. and Wilcox, L.: Emerging Asian aerosol patterns, Nat. Geosci., 12, 582-584, https://doi.org/10.1038/s41561-019-0424-5, 2019.

Sperber, K. R., Annamalai, H., Kang, I. S., Kitoh, A., Moise, A., Turner, A., Wang, B. and Zhou, T.: The Asian summer monsoon: an intercomparison of CMIP5 vs. CMIP3 simulations of the late 20th century, Clim. Dynam., 41, 2711-2744, 10.1007/s00382-012-1607-6, 2013.

Stier, P., van den Heever, S. C., Christensen, M. W., Gryspeerdt, E., Dagan, G., Saleeby, S. M., Bollasina, M., Donner, L., Emanuel, K., Ekman, A. M. L., Feingold, G., Field, P., Forster, P. and Haywood, J.: Multifaceted Aerosol Effects on Precipitation, Nat. Geosci., 17, 719-732, https://doi.org/10.1038/s41561-024-01482-6, 2024.

Stjern, C. W., Samset, B. H., Myhre, G., Forster, P. M., Hodnebrog, Ø, Andrews, T., Boucher, O., Faluvegi, G., Iversen, T., Kasoar, M., Kharin, V., Kirkevåg, A., Lamarque, J.-F., Olivieì, D., Richardson, T., Shawki, D., Shindell, D., Smith, C., Takemura, T. and Voulgarakis, A.: Rapid adjustments cause weak surface temperature response to increased black carbon concentrations, J. Geophys. Res.-Atmos., 122, 11462-1481, https://doi.org/10.1002/2017JD027326, 2017.

Stjern, C., Joshi, M., Wilcox, L., Gollo, A. and Samset, B.: Systematic Regional Aerosol Perturbations (SyRAP) in Asia using the intermediate-resolution global climate model FORTE2, J. Adv. Mod. Earth System, accepted, 2024.

Tian, F., Dong, B., Robson, J. and Sutton, R.: Forced decadal changes in the East Asian

summer monsoon: the roles of greenhouse gases and anthropogenic aerosols, Clim. Dynam., https://doi.org/10.1007/s00382-018-4105-7, 2018.

Wang, H.: The weakening of the Asian monsoon circulation after the end of 1970's, Adv. Atmo. Sci., 18, 376-386, https://doi.org/10.1007/BF02919316, 2001.

Wang, Z., Lin, L., Yang, M., Xu, Y. and Li, J.: Disentangling fast and slow responses of the East Asian summer monsoon to reflecting and absorbing aerosol forcings, Atmos. Chem. Phys., 17, 11075-11088, https://doi.org/10.5194/acp-17-11075-2017, 2017.

Webb, D. J.: An ocean model code for array processor computers, Comput. Geosci., 22, 569-578, 1996.

Westervelt, D. M., Conley, A. J., Fiore, A. M., Lamarque, J.-F., Shindell, D. T., Previdi, M., Mascioli, N. R., Faluvegi, G., Correa, G., and Horowitz, L. W.: Connecting regional aerosol emissions reductions to local and remote precipitation responses, Atmos. Chem. Phys., 18, 12461-12475, https://doi.org/10.5194/acp-18-12461-2018, 2018.

Westervelt, D. M., You, Y., Li, X., Ting, M., Lee, D. and Ming, Y.: Relative importance of greenhouse gases, sulfate, organic carbon, and black carbon aerosol for South Asian monsoon rainfall changes, Geophys. Res. Lett., 47, e2020GL088363, https://doi.org/10.1029/2020GL088363, 2020.

Wilcox, L. J., Dong, B., Sutton, R. T., Highwood, E. J.: The 2014 Hot, Dry Summer in Northeast Asia, Bull. Amer. Meteor. Soc., 96, 105-110, https://doi.org/10.1175/BAMS-D-15-00123.1, 2015.

Wilcox, L. J., Liu, Z., Samset, B. H., Hawkins, E., Lund, M. T., Nordling, K., Undorf, S., Bollasina, M., Ekman, A. M. L., Krishnan, S., Merikanto, J., and Turner, A. G.: Accelerated increases in global and Asian summer monsoon precipitation from future aerosol reductions, Atmos. Chem. Phys., 20, 11955–11977, https://doi.org/10.5194/acp-20-11955-2020, 2020.

Xiang, B., Xie, S. P., Kang, S. M., and Kramer, R.: An emerging Asian aerosol dipole pattern reshapes the Asian summer monsoon and exacerbates northern hemisphere warming, npj Clim. Atmos. Sci., 6, 77, https://doi.org/10.1038/s41612-023-

926   00400-8, 2023.

927   Xie, X., Myhre, G., Liu, X., Li, X., Shi, Z., Wang, H., Kirkevåg, A., Lamarque, J. F.,

928   Shindell, D., Takemura, T., and Liu, Y.: Distinct responses of Asian summer

929   monsoon to black carbon aerosols and greenhouse gases, Atmos. Chem. Phys., 20,

930   11823-11839, https://doi.org/10.5194/acp-20-11823-2020, 2020.

931   Yang, J., Kang, S., Chen, D., Zhao, L., Ji, Z., Duan, K., Deng, H., Tripathee, L., Du, W.,

932   Rai, M., Yan, F., Li, Y. and Gillies, R.: South Asian black carbon is threatening the

933   water sustainability of the Asian Water Tower, Nat. Commun., 13, 7360,

934   https://doi.org/10.1038/s41467-022-35128-1, 2022.

935   Zhang, H., Wang, Z., Guo, P., and Wang, Z.: A modeling study of the effects of direct

936   radiative forcing due to carbonaceous aerosol on the climate in East Asia, Adv.

937   Atmos. Sci., 26, 57-66, https://doi.org/10.1007/s00376-009-0057-5, 2009.

938   Zhong, W. Y. and Haigh, J. D.: Improved broad-band emissivity parameterization for

939   water vapor cooling calculations, J. Atmos. Sci., 52, 124-148, 1995.

940

941   **Table 1.** Summary of SyRAP-FORTE2 simulations used in the study

Experiment[a]	Name	Aerosol	Region	GHG	Years
Baseline	piC	No aerosol	--	Preindustrial climate conditions (280 ppmv)	200
Perturbation	BC_CHI	Added BC[b]	East China (95-133°E, 20-53°N)		
	BC_IND		India (65-95°E, 5-35°N)		
	BC_CHI+IND		both East China and India region		

942   a. only ARI effect is considered

943   b. CAMSRA monthly climatology of BC AOD for 2003-2021

944
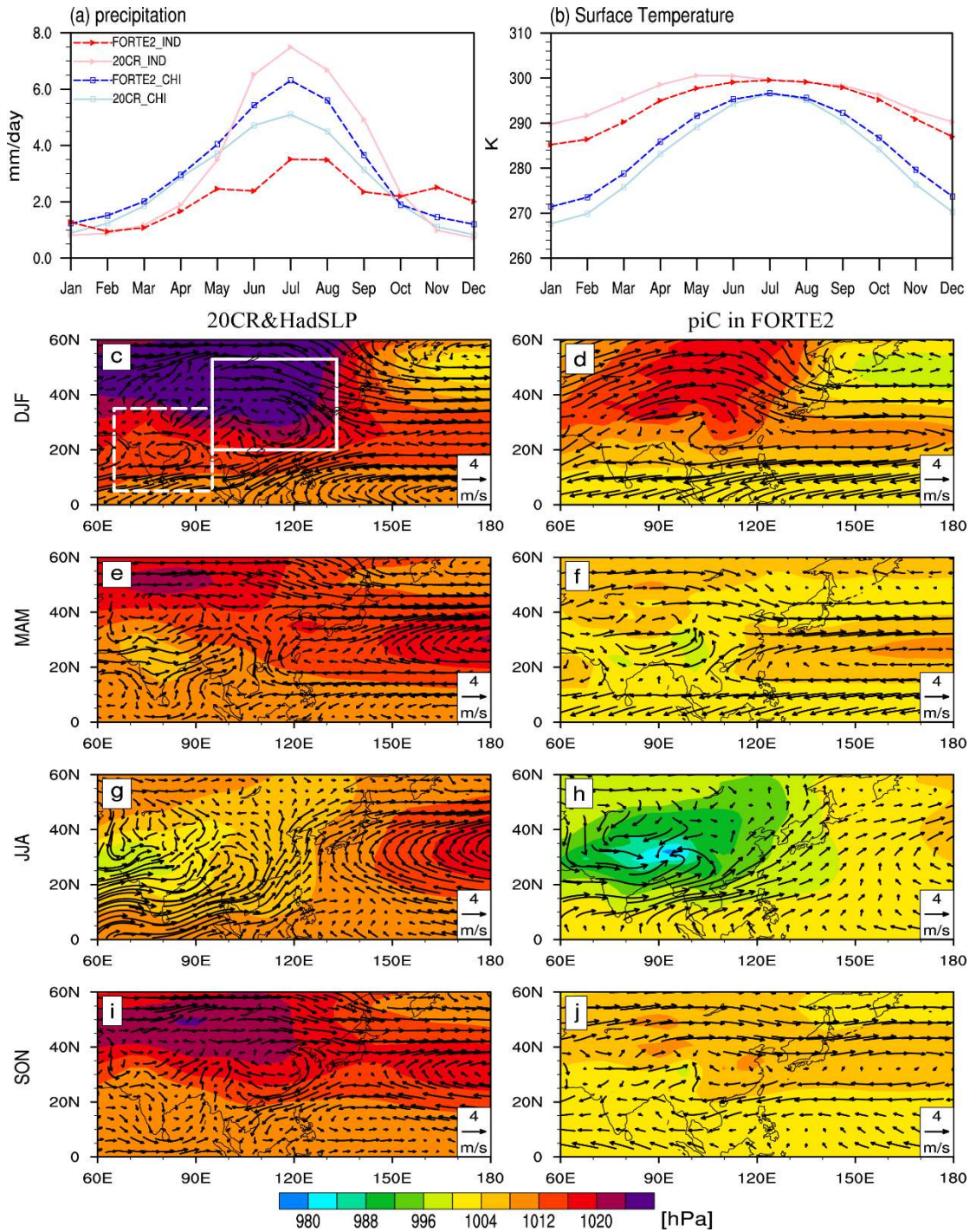
945 **Figure 1.** Seasonal evolutions of (a) the regional mean precipitation (unit: mm/day) of

946 20CR (solid lines) and the baseline simulation of FORTE2 (dashed lines) for East Asia

947 (95°E-133°E, 20°N-53°N, the solid, white box in (c)) (light blue and blue lines), and

948 India (65°E-95°E, 5°N-35°N, the dashed, white box in (c)) (pink and red lines). (b)

949 same as (a), but for surface temperature (unit: K). Climate state of SLP (unit: hPa) and

950 850 hPa horizontal winds (unit: m/s) in (left) 20CR and HadSLP and (right) the baseline

951 simulation of FORTE2 in four seasons (c-j).
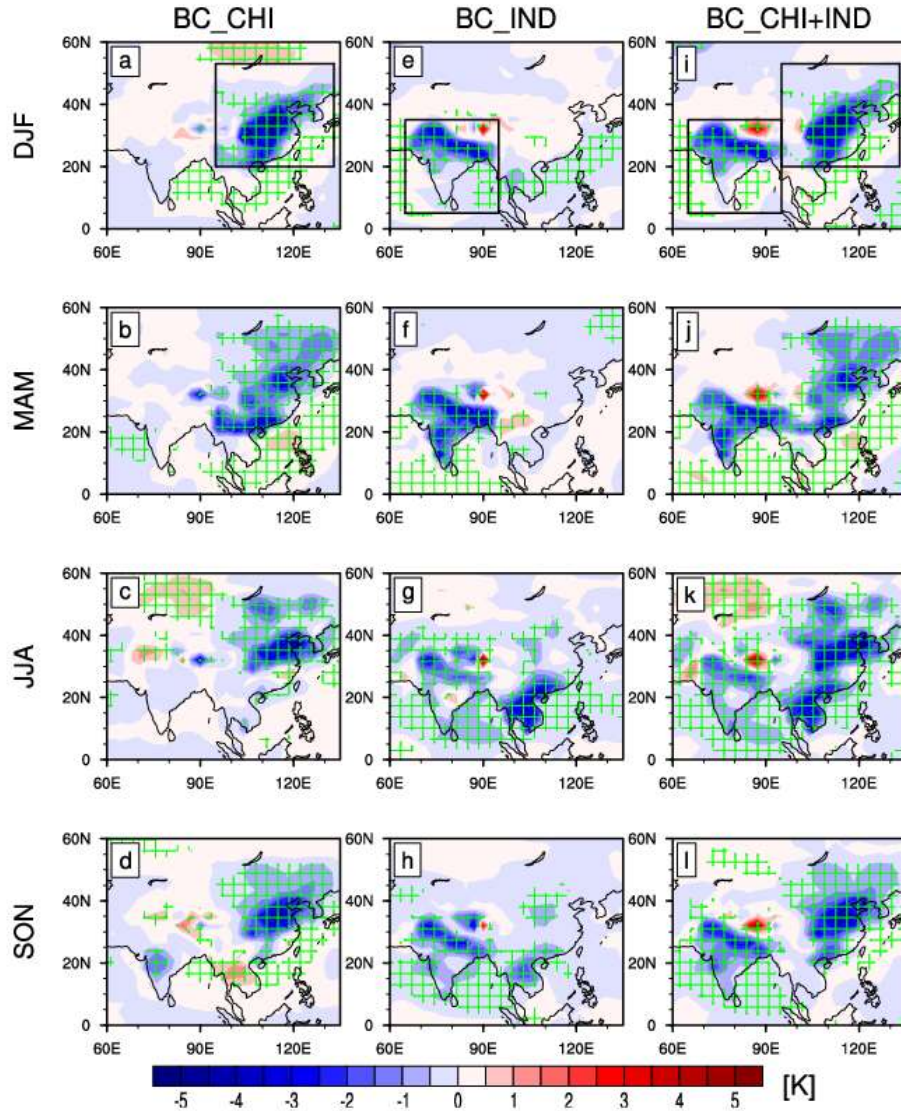
Figure 2. Spatial patterns of Ts responses in (a-d) BC_CHI, (e-h) BC_IND, and (i-l) BC_CHI+IND for four seasons. The green gridlines indicate the regions where the responses are statistically significant above 95% level based on a two-tailed Student's t-test. The black boxes in (a), (e) and (i) highlight the region where BC aerosols are perturbed. Unit: K
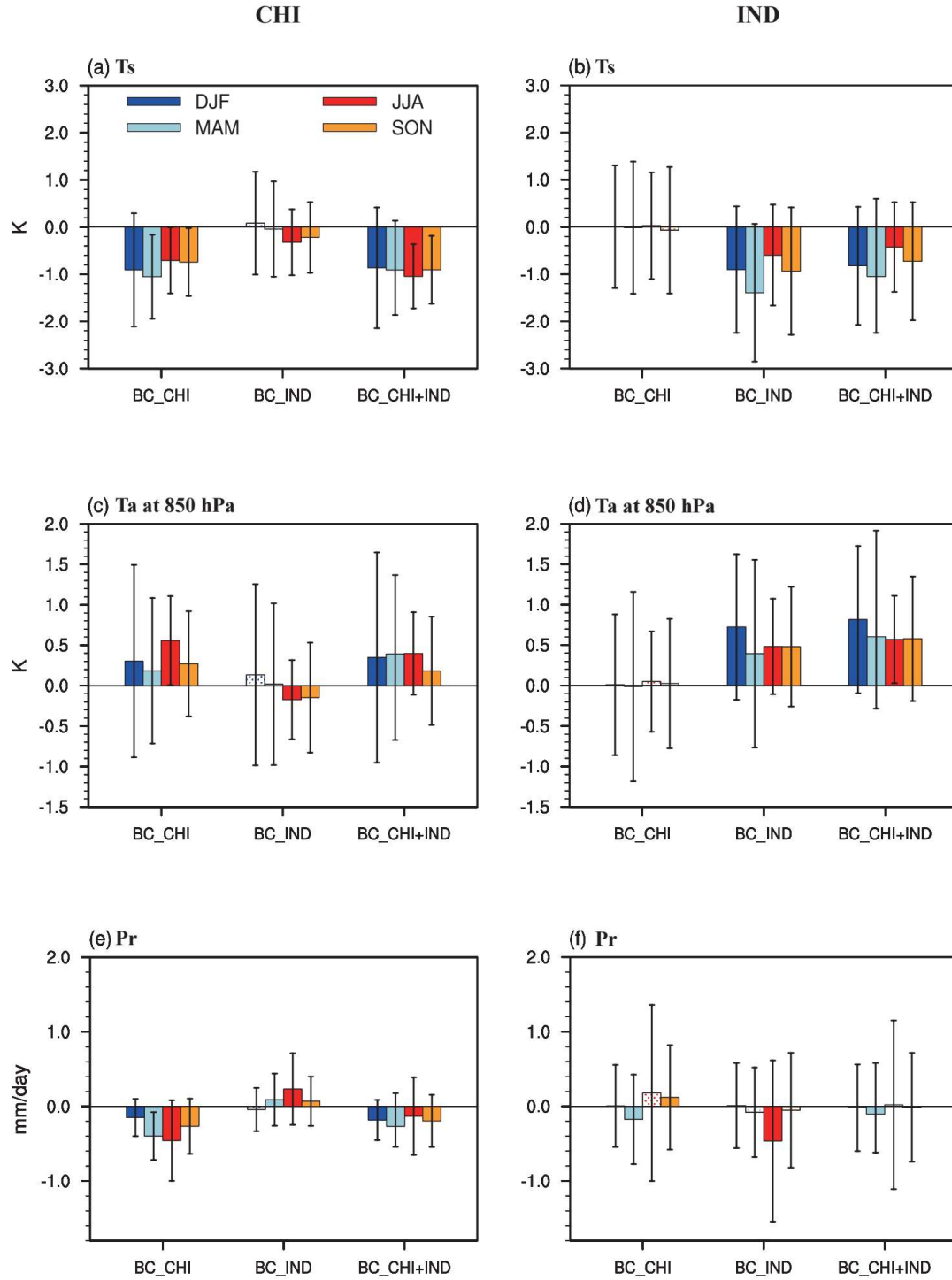
Figure 3. Area-averaged land responses of (a-b) Ts, (c-d) Ta at 850 hPa, and (e-f) precipitation over East China (CHI: 95°E-133°E, 20°N-53°N) and India (IND: 65°E-95°E, 5°N-35°N) for four seasons (DJF: blue bars, MAM: light blue bars, JJA: red bars, and SON: yellow bars). Solid bars indicate the responses are statistically significant above 95% level based on a two-tailed Student's t-test. Error bars represent ±1 standard deviations of the response.
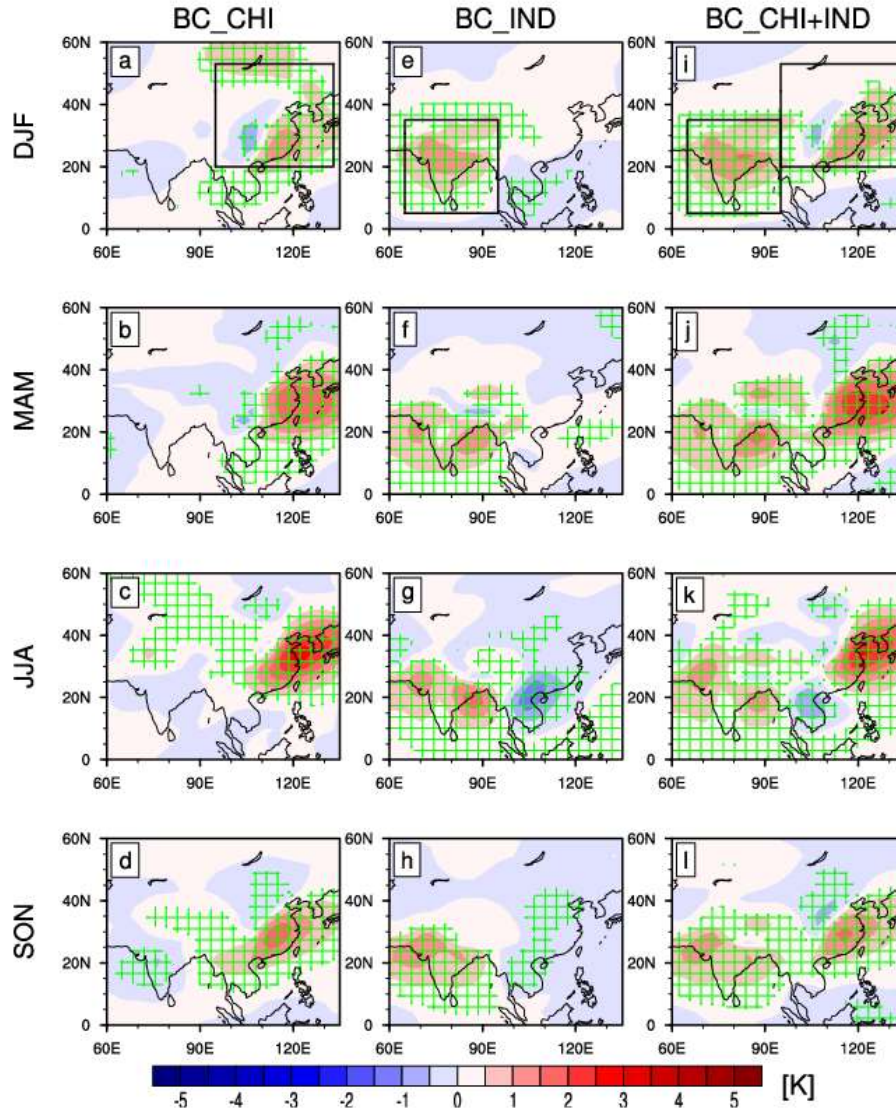
Figure 4. Spatial patterns of Ta responses at 850 hPa in (a-d) BC_CHI, (e-h) BC_IND, and (i-l) BC_CHI+IND for four seasons. The green gridlines indicate the regions where the responses are statistically significant above 95% level based on a two-tailed Student's t-test. The black boxes in (a), (e) and (i) highlight the region where BC aerosols are perturbed. Unit: K

971
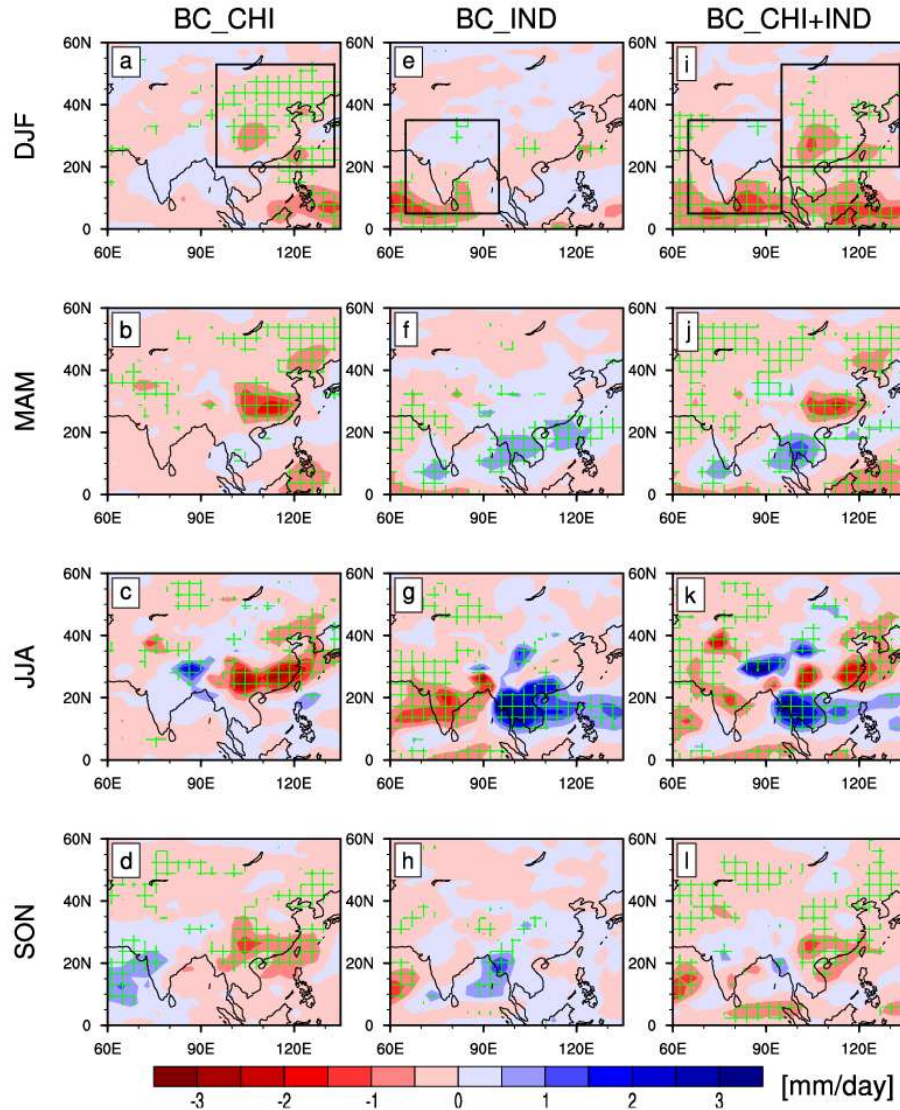
Figure 5. Spatial patterns of precipitation responses in (a-d) BC_CHI, (e-h) BC_IND, and (i-l) BC_CHI+IND for four seasons. The green gridlines indicate the regions where the responses are statistically significant above 95% level based on a two-tailed Student's t-test. The black boxes in (a), (e) and (i) highlight the region where BC aerosols are perturbed. Unit: mm/day

977

978
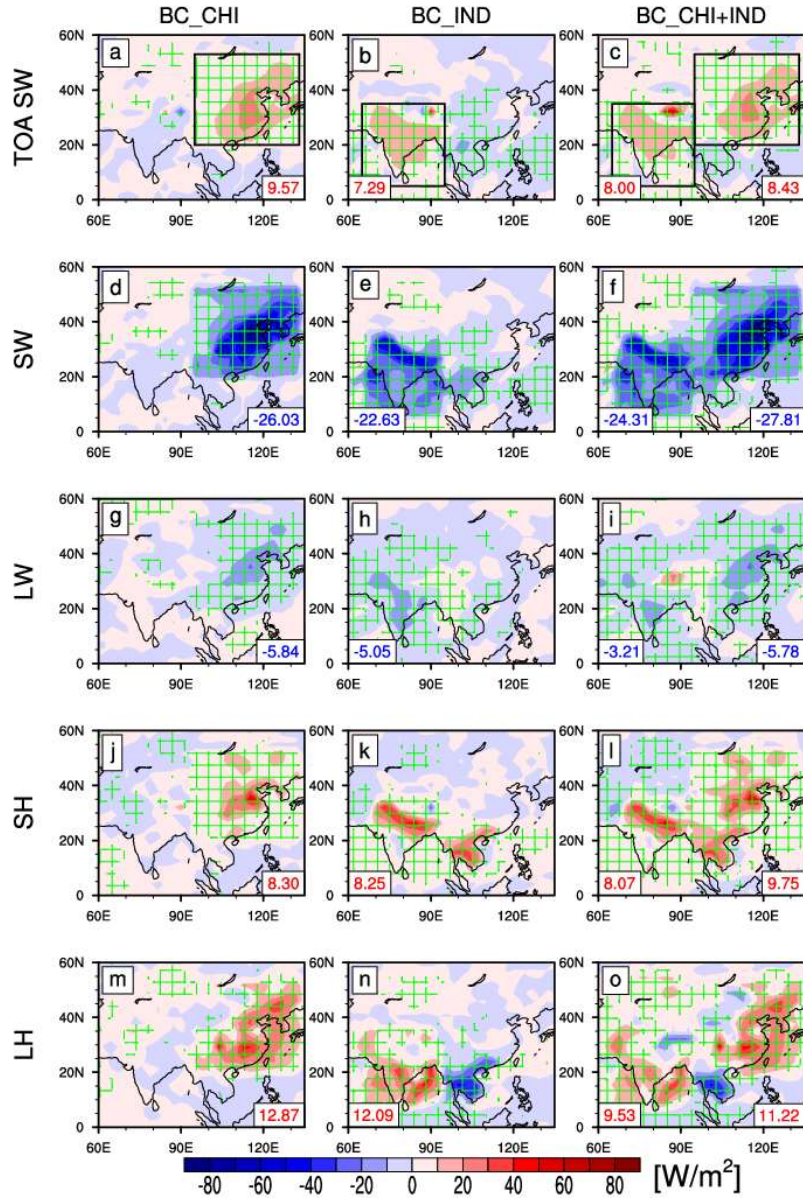
Figure 6. Spatial patterns of net TOA and surface energy responses in summer in BC_CHI, BC_IND, and BC_CHI+IND, respectively. (a-c) TOA SW, (d-f) surface SW, (g-i) surface LW, (j-l) surface SH, and (m-o) surface LH. Positive values mean downward for radiation and flux changes. Area-averaged values over East China and India are given in the lower right corners and lower left corners, respectively. The green gridlines indicate the regions where the responses are statistically significant above 95% level based on a two-tailed Student's t-test. The black squares highlight the regions where BC are perturbed. Units: W/m^2

987
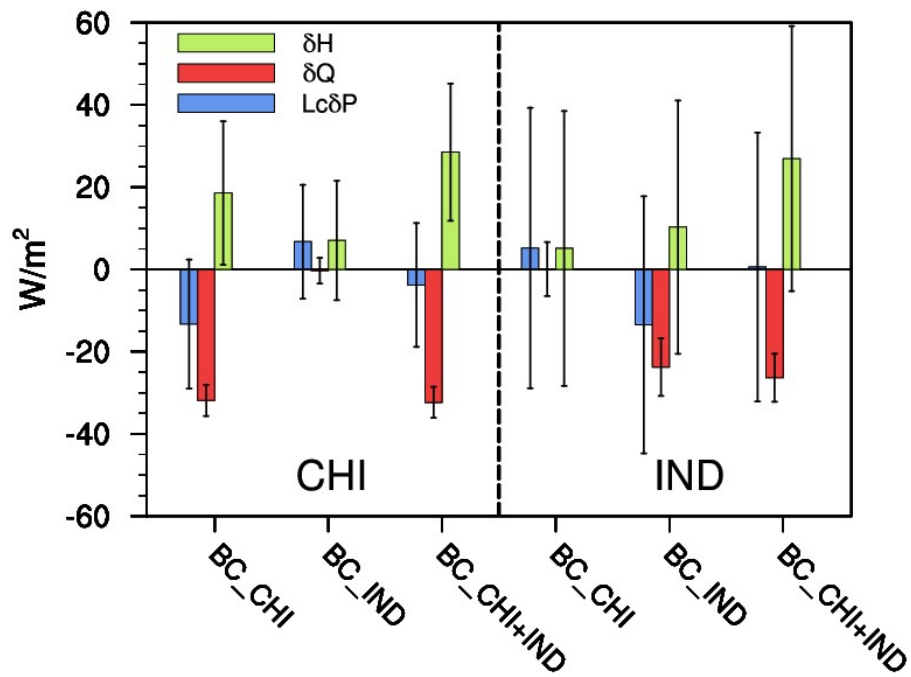
Figure 7. Summer area-averaged responses of the atmospheric energy budget terms over East China (CHI: 95°E-133°E, 20°N-53°N) and India (IND: 65°E-95°E, 5°N-35°N) in BC_CHI, BC_IND, and BC_CHI+IND. Error bars represent ±1 standard deviations of the response. Unit: W/m^2

992
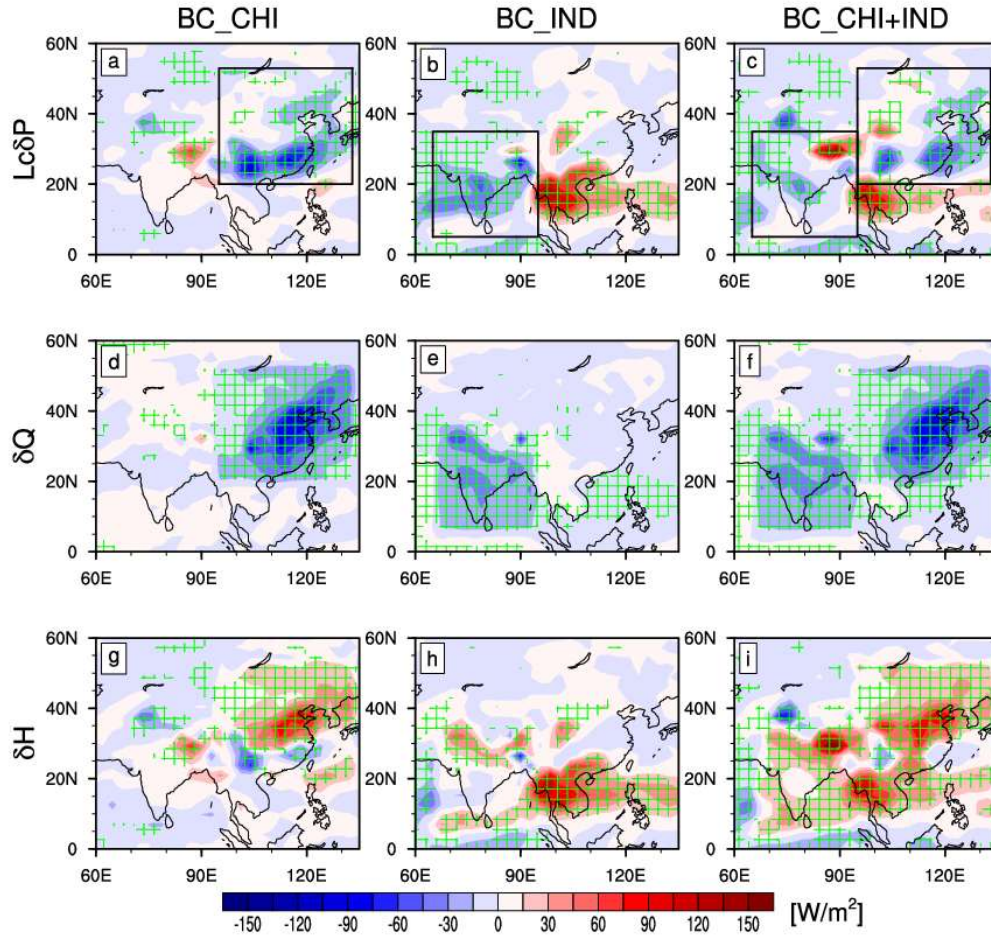
Figure 8. Summer spatial patterns of responses of the atmospheric energy budget terms

in BC_CHI, BC_IND, and BC_CHI+IND. (a-c) $L_c\delta P$, (d-f) δQ and (g-i) δH. The green

gridlines indicate the regions where the responses are statistically significant above 95%

level based on a two-tailed Student's t-test. The black squares highlight the regions

where BC are perturbed. Unit: W/m^2

998
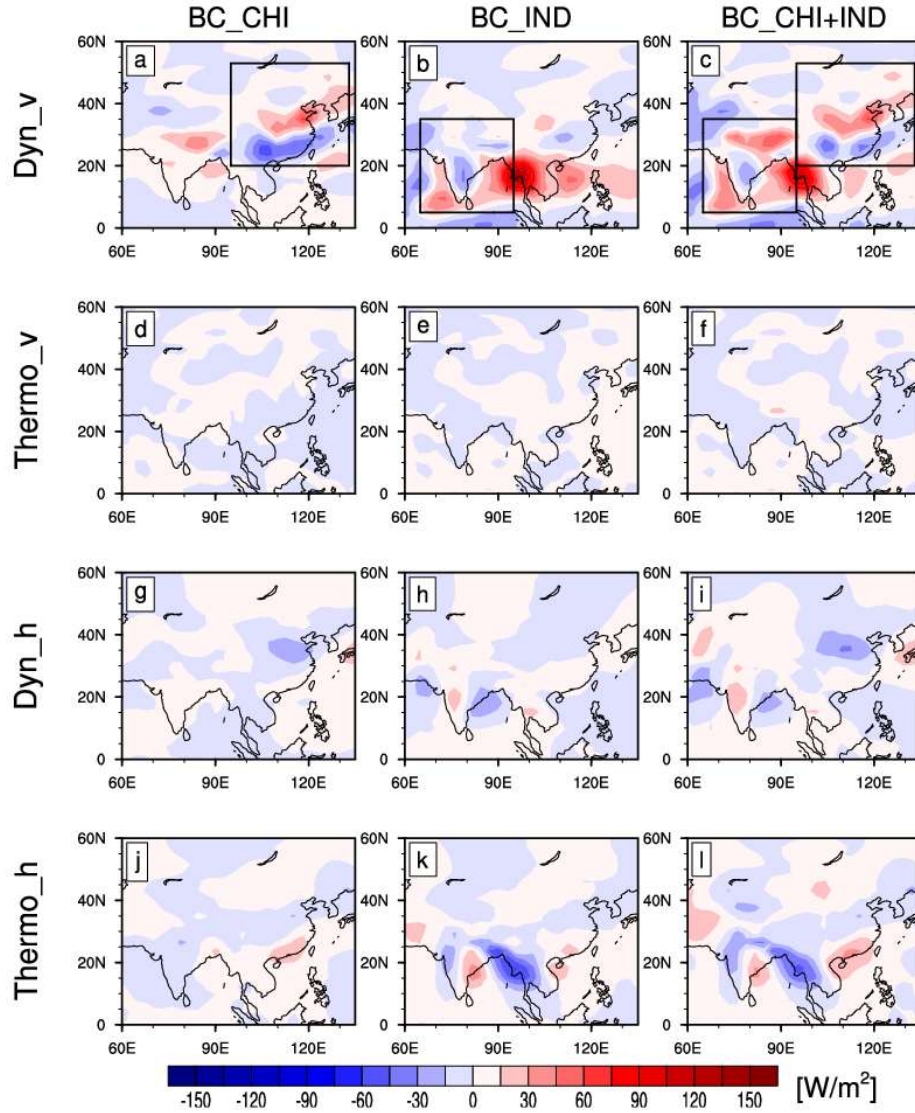
Figure 9. Summer spatial patterns of responses in the four terms decomposed by δH_m in BC_CHI, BC_IND, and BC_CHI+IND. (a-c) the dynamic components with changes in vertical atmospheric circulations (δH_{Dyn_v}), (d-f) the thermodynamic components with changes in vertical atmospheric circulations (δH_{Thermo_v}), (g-i) dynamic components with changes in horizontal DSE gradients (δH_{Dyn_h}), and (j-l) thermodynamic components with changes in horizontal DSE gradients (δH_{Thermo_h}) The black squares highlight the regions where BC are perturbed. Unit: W/m^2

1006

1007
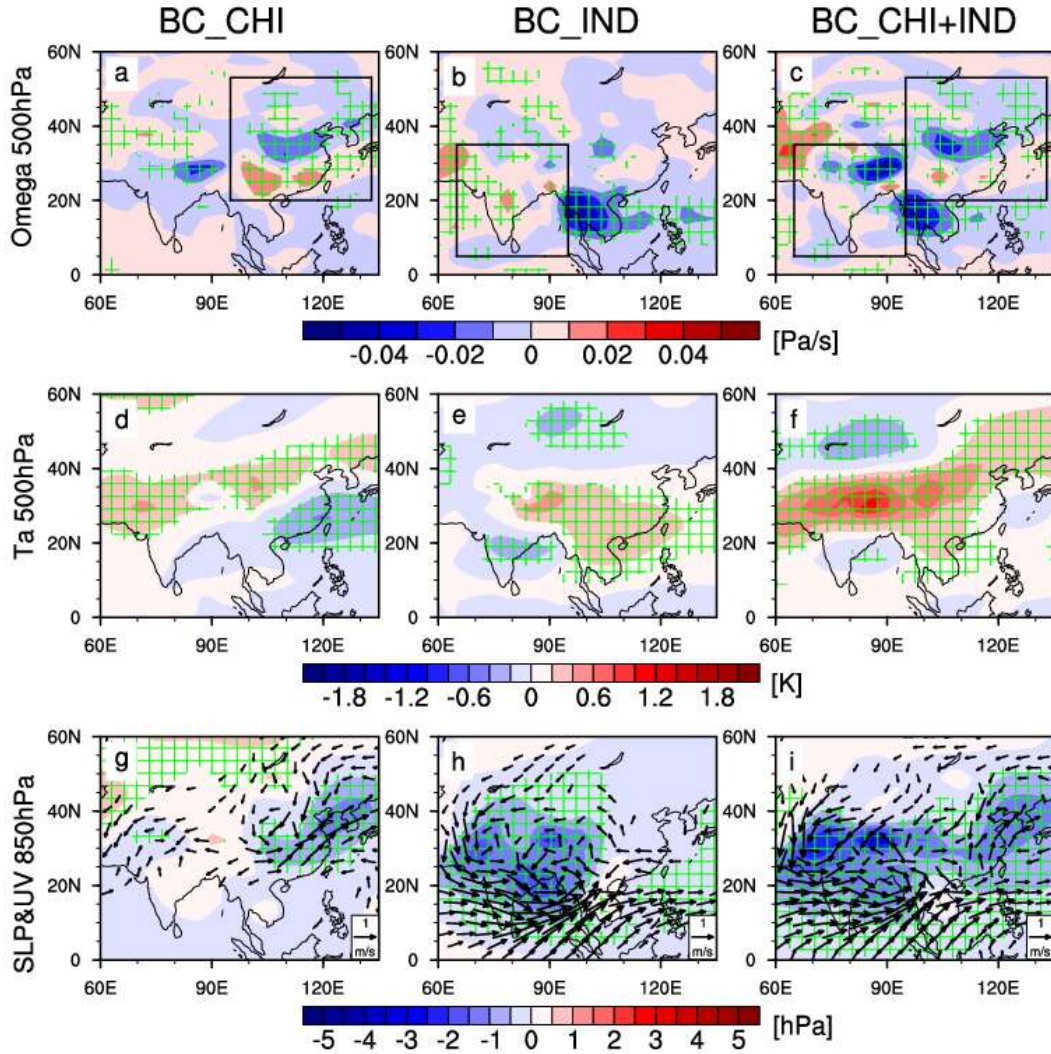
Figure 10. Summer spatial patterns of responses in (a-c) Omega at 500 hPa (Unit: Pa/s), (d-f) Ta at 500 hPa (Unit: K), and (g-i) SLP (Unit: hPa) and horizontal wind at 850 hPa (Unit: m/s) in BC_CHI, BC_IND and BC_CHI+IND. The green gridlines indicate the regions where the responses are statistically significant above 95% level based on a two-tailed Student's t-test. Wind vectors are only shown for grid boxes where at least one component of the wind significant above the 95% level are shown. The black squares highlight the regions where BC are perturbed.
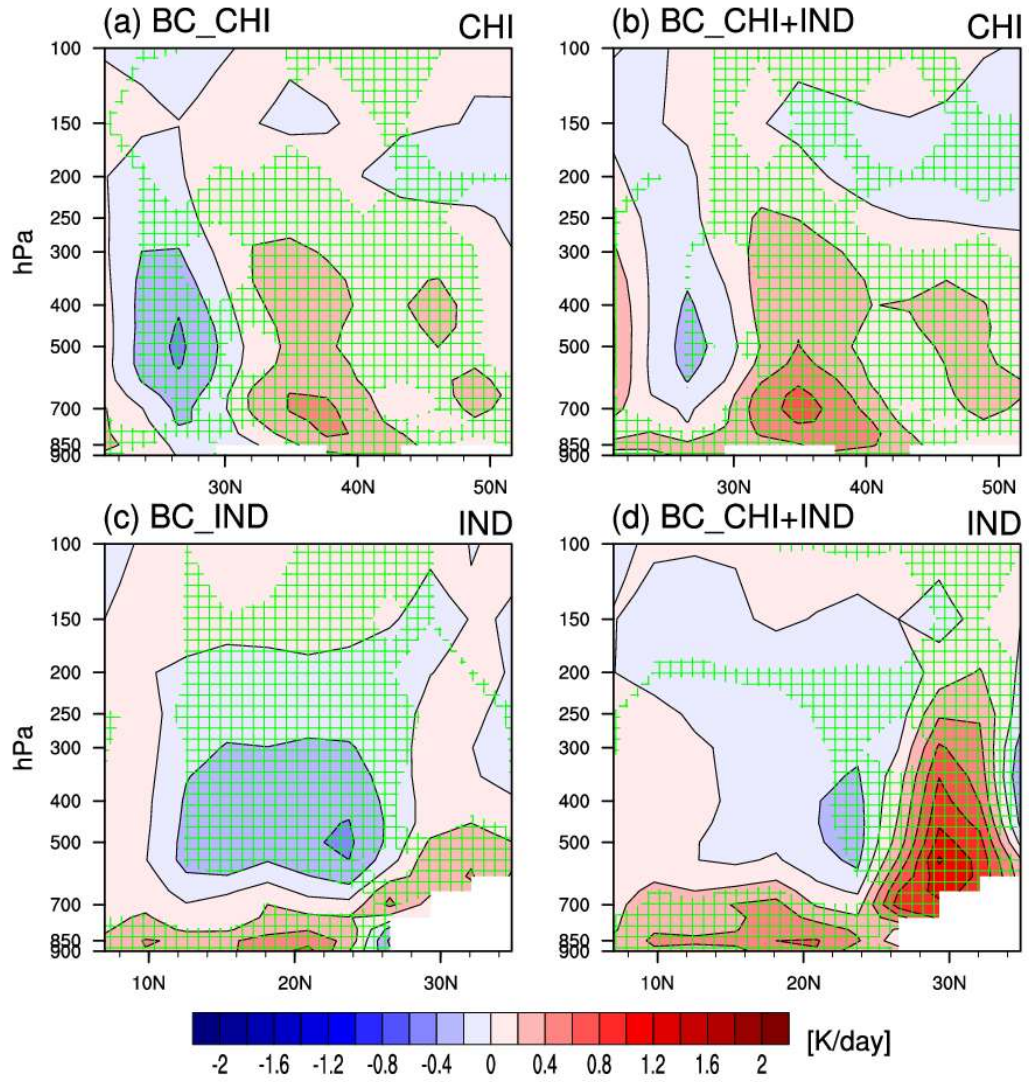
Figure 11. Zonal mean of diabatic heating responses averaged over (a-b) East China (95°E-133°E, the black square in Fig.10a) for BC_CHI and BC_CHI+IND, and over (c-d) India (65°E-95°E, the black square in Fig.10b) for BC_IND and BC_CHI+IND in summer. The green gridlines indicate the regions where the responses are statistically significant above 95% level based on a two-tailed Student's t-test. The white part indicates a symbol of topography. Unit: K/day

1022

1023
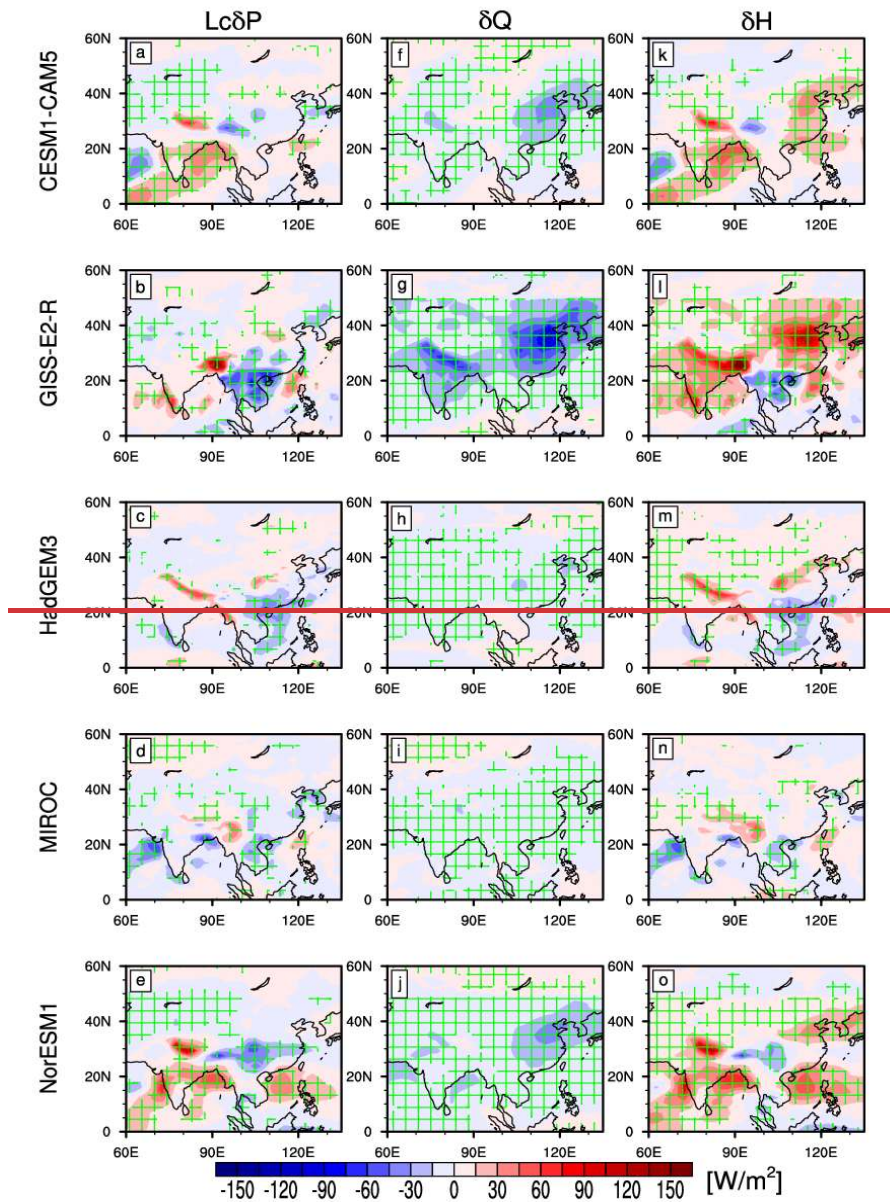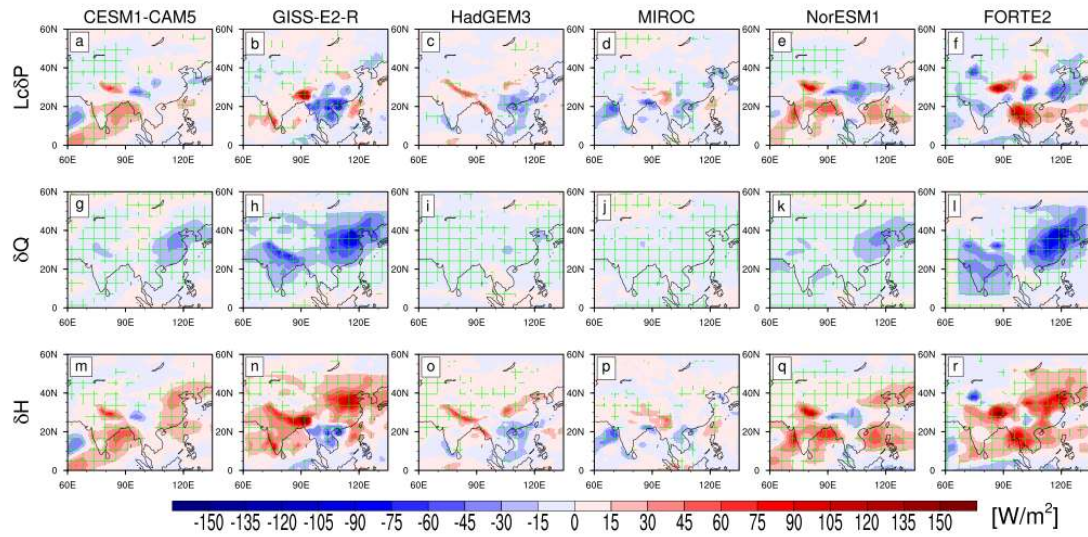
1024 **Figure 12.** Summer spatial patterns of responses of the atmospheric energy budget

1025 terms in the five PDRMIP models and the BC_CHI+IND simulation in FORTE2. (a-e)

1026 $L_c\delta P$, (f-j) δQ and (k-o) δH. The green gridlines indicate the regions where the

1027 responses are statistically significant above 95% level based on a two-tailed Student's

1028 t-test. Unit: W/m^2

1029
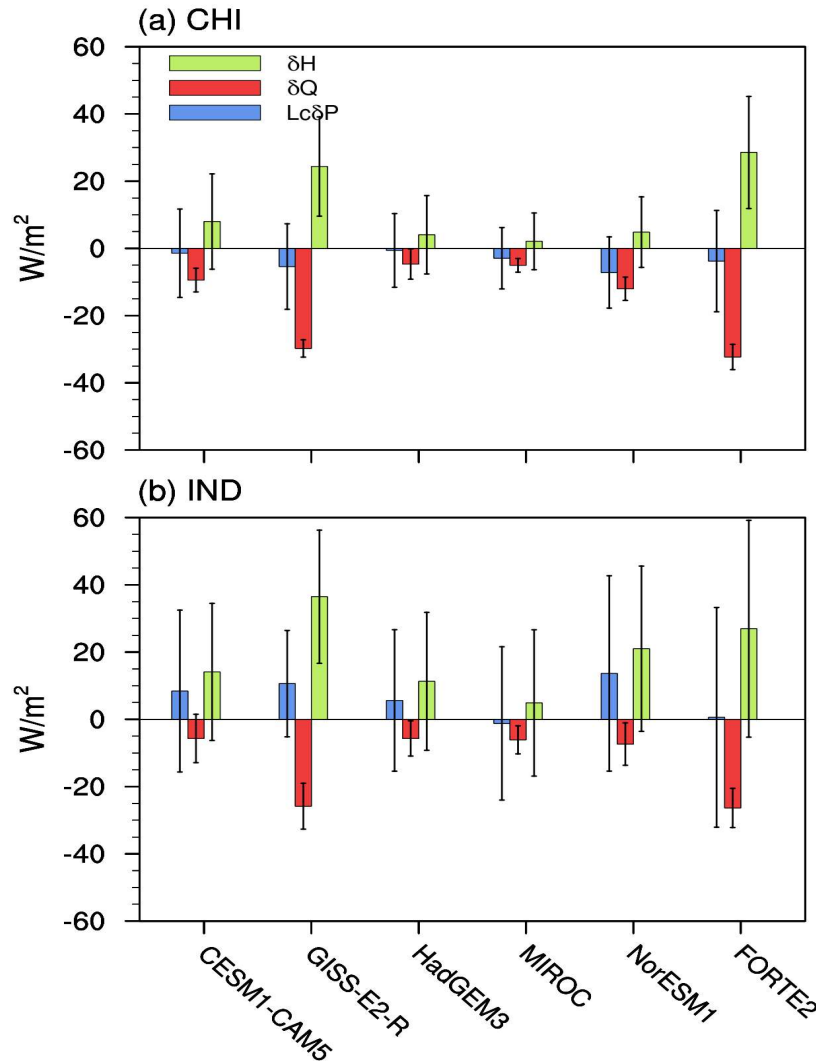
1030 **Figure 13.** Summer area-averaged responses of the atmospheric energy budget terms

1031 over (a) East China (CHI: 95°E-133°E, 20°N-53°N) and (b) India (IND: 65°E-95°E,

1032 5°N-35°N) in the five PDRMIP models and the BC_CHI+IND simulation in FORTE2.

1033 Error bars represent ±1 standard deviations of the response. Unit: W/m^2